[AMERICAN JOURNAL OF SCIENCE, VOL. 282, SUMMER, 1982, P. 970-1011]

REACTION SKARNS BETWEEN QUARTZ-BEARING AND OLIVINE-BEARING ROCKS

RICHARD O. SACK*

Department of Geological Sciences, Hoffman Laboratory,
Harvard University, 20 Oxford Street,
Cambridge, Massachusetts 02138

ABSTRACT. *Chemical zoning patterns, mineral assemblages, and reaction textures in orthopyroxene-bearing reaction skarns adjacent to a quartz vein and a plagioclase–quartz dike have been used to deduce chemical potential gradients and to examine the reactions that have led to the present distribution of assemblages. Orthopyroxene is developed in metasomatic zones that separate quartz-bearing and fosteritic olivine-bearing rocks in the core of a layered metagabbro body on the eastern edge of the Precambrian of the Adirondack highlands, New York. Developed in country rocks which record temperatures and pressures of 730 ± 50°C and 8 ± 1 kb for a Grenville metamorphic event, these skarns provide examples of extreme disequilibrium. For example, adjacent to a quartz vein is a skarn about 1.5 cm wide in which orthopyroxenes exhibit a change in Fe/(Fe + Mg) of 0.34 to 0.55 from contact with olivine to contact with quartz. Across a section of this skarn average chemical potential gradients are calculated to have been 0.03 ± 0.3, −0.47 ± 0.17, −1.90 ± 0.20, ≤ −2.5 ± 0.1, and + 1.28 ± 0.15 kcal/cm for oxide components CaO, FeO, MgO, $AlO_{3/2}$, and SiO_2, respectively, at the conditions of local metamorphic equilibration with directions toward the core of the vein taken as positive. The magnitudes of the gradients of these oxide components, together with mass-balance considerations based on inert markers, extrema in chemical profiles at the wall of the quartz vein, and the reaction textures within the skarns, indicate the following relative mobilities for these components: $CaO \geqslant FeO > MgO > SiO_2 > AlO_{3/2}$. Core to rim variations in Fe/(Fe + Mg) ratios of olivines and orthopyroxenes near olivine-orthopyroxene and orthopyroxene-quartz layer contacts suggest that the differences between Fe/(Fe + Mg) ratios of orthopyroxenes at these contacts became greater with time. The inferred changes in Fe/(Fe + Mg) zoning patterns within the olivine–orthopyroxene–quartz subsystem of this skarn may be interpreted as due to either retrograde cooling or polymetamorphism, because the bounding layer contact assemblages are only bivariant even within the model system MgO–FeO–SiO_2. These inferences are consistent with those based on the analysis of garnet-bearing corona structures in the country rocks and garnet-forming reactions within the skarns.*

INTRODUCTION

The importance of grain-boundary diffusion as a mechanism of mass transfer during metamorphic reactions has been emphasized in several recent contributions. These studies have focused on developing diffusion models to account for reaction structures ranging from microscopic mineral segregations (Carmichael, 1969; Eugster, 1970; Fisher, 1970, 1973; Whitney and McLelland, 1973; Weare, Stephens, and Eugster, 1976) to

* Present address: Department of Geosciences, Purdue University, West Lafayette, Indiana 47907

reaction skarns developed between incompatible rock units. Examples of the latter include blackwall and talc-carbonate reaction skarnes and envelopes between serpentinized peridotite bodies and quartzo-feldspathic gneisses (Phillips and Hess, 1936; Curtis and Brown, 1969; Carswell, Curtis, and Kanaris- Sotiriou, 1974; Frantz and Mao, 1976; Brady, 1977; Sanford, ms), the high temperature reaction skarns and aureoles between quartz-bearing rock and marble or mafic magma (Read, 1931; Barker, 1964; Joesten, 1974), and calc-silicate reaction skarns produced at the contacts of marble and pelite during regional metamorphism (Orville, 1969; Vidale and Hewitt, 1973; Thompson, 1975; Brady, 1977).

In their treatments of diffusion, most of these studies have made use of the assumption of local equilibrium (Korzhinskii, 1959; Thompson, 1959). With this assumption, chemical potential gradients in the intergranular medium have been calculated to document the magnitude of the energy differences responsible for diffusion (for example, Korzhinskii, 1959; Vidale, 1969; Fisher, 1970; Shay, 1975; Sanford, ms). In addition, the formalism of nonequilibrium thermodynamics has been developed and applied to diffusion in mineral segregations and skarns (for example, Fisher, 1973). Using this formalism Fisher (1977) and Joesten (1977) have shown how the assumption of quasi-steady state diffusion, "(1) that the diffusing species are everywhere in local equilibrium with the adjacent minerals, so that the rate of the overall process depends on the rate of diffusion; and (2) that the fluxes and potential gradients within the system will continually adjust to values closely approximating those of a steady state" (Fisher and Elliot, 1974, p. 231-232), may be used to predict mineral zoning sequences and modal abundances in order to constrain relative diffusion coefficients for a variety of reaction textures. These studies have focused on systems composed of endmember minerals at constant temperature and pressure.

This paper examines the orthopyroxene-bearing reaction skarns developed between feldspathic cumberlandite (olivine–plagioclase–magnetite–ilmenite rock), a plagioclase-quartz dike, and an associated quartz vein. The occurrences described are found in a metagabbro body from the eastern edge of the Precambrian Adirondack highlands near Westport, N.Y. (Kemp, 1894; Buddington and Whitcomb, 1941; Sack, ms). Within this body, cumberlandite is found in two Fe-Ti oxide-rich layers in the largely undeformed metagabbro core where primary magmatic layering is preserved. The dike and vein that cross cut these layers occur in an adit that forms part of the now abandoned workings of the Splitrock magnetite mine (Kemp, 1894). The two reaction skarns described here were obtained near the entrance to the northernmost adit. The petrology of the country rocks of these reaction skarns has been described in detail by Sack (ms and 1980b). Mineral assemblages in the country rocks record temperatures and pressures of local metamorphic equilibration of 730 ± 50°C and 8 ± 1 kb for a Grenville event (Sack, 1977). These estimates are in accord with those obtained by Bohlen and Essene (1980) for areas bordering this locality.

These orthopyroxene-bearing reaction skarns are of interest, because they provide examples of extreme disequilibrium which is the result of the well known incompatibility between magnesian olivine and quartz. In contrast to hypothetical skarns composed of endmember minerals, much of the disequilibrium recorded in one of the skarns is expressed by continuous variations in the compositions of solid solution phases (particularly orthopyroxene and plagioclase) within the intergranular network. Superimposed on these continuous composition variations are prominent iron-magnesium zoning patterns in grains of olivine and orthopyroxene near the edges of the orthopyroxene-bearing reaction skarn. In this paper inert markers and compositional variations within the intergranular network will be used to assess the relative mobilities of oxide components CaO, FeO, MgO, $AlO_{3/2}$, and SiO_2. Models will be developed to relate the evolution of zoning patterns within the skarns to changes in temperature and pressure conditions.

PETROGRAPHY

The two orthopyroxene-bearing reaction skarns described here separate olivine-bearing from quartz-bearing rocks. In this discussion the terms inner and outer side will be used to designate directions toward and away from the quartz-bearing vein or dike, the term inner interface will be used to designate the contact surface between the orthopyroxene-bearing reaction skarn and the quartz vein or plagioclase-quartz dike, and the term outer interface will be used to designate the contact surface between the orthopyroxene-bearing reaction skarn and the olivine-bearing country rock. Some of the petrologic details of these reaction skarns are shown in plate 1 and figures 1 and 2. The quartz vein is nowhere more than 1.5 cm thick and is presently composed of roughly equant quartz grains extending across the vein. Its reaction skarn is less than 2 cm thick. The plagioclase-quartz dike is between 10 to 18 cm thick and lacks quartz at its margins. The olivine-bearing country rock for these skarns is a feldspathic variant of cumberlandite. Cumberlandite is a rock composed predominantly of olivine and Fe-Ti oxides magnetite and ilmenite with about 15 percent plagioclase laths (compare Johnson and Warren, 1908). Cumberlandite is commonly developed as magmatic layers in layered basic intrusions, although it is typically not designated as such. The cumberlandite and feldspathic cumberlandites that form the country rocks for the reaction skarns are approximately linear mixtures of the following rock types: (1) olivine and Fe-Ti oxides in approximate volume proportions 2:1 and (2) olivine, plagioclase, and Fe-Ti oxides in approximate volume proportions 2:1:1 and variable hornblende. Although there is evidence in the country rocks that some of the hornblende is secondary and some clinopyroxene is primary, mass balance considerations in the feldspathic cumberlandites (Sack, ms), at least, suggest that much of the hornblende is primary. This mineral assemblage has been further augmented by the development of secondary metamorphic minerals: garnet, spinel, biotite, ilmenite, and hornblende.

PLATE 1

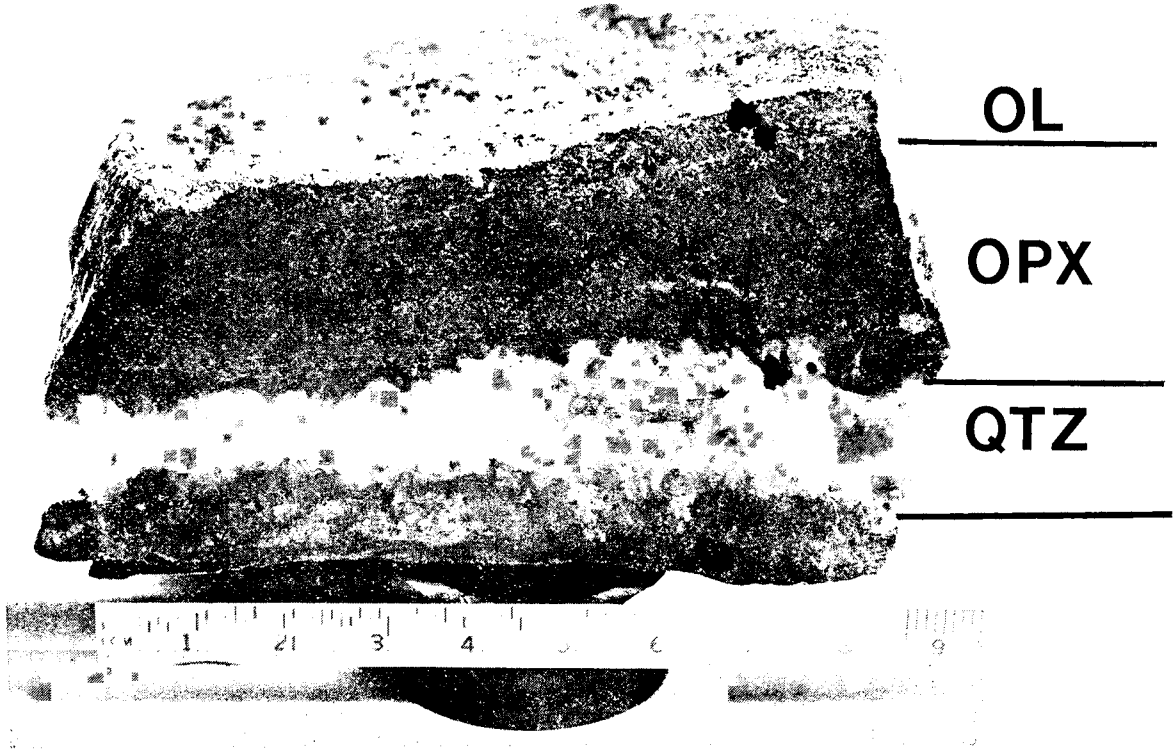

Hand specimen with skarn between a quartz vein (QTZ) and an olivine–hornblende–magnetite–ilmenite–spinel–biotite rock (OL). The zone adjacent to the vein is composed almost exclusively of orthopyroxene (OPX).

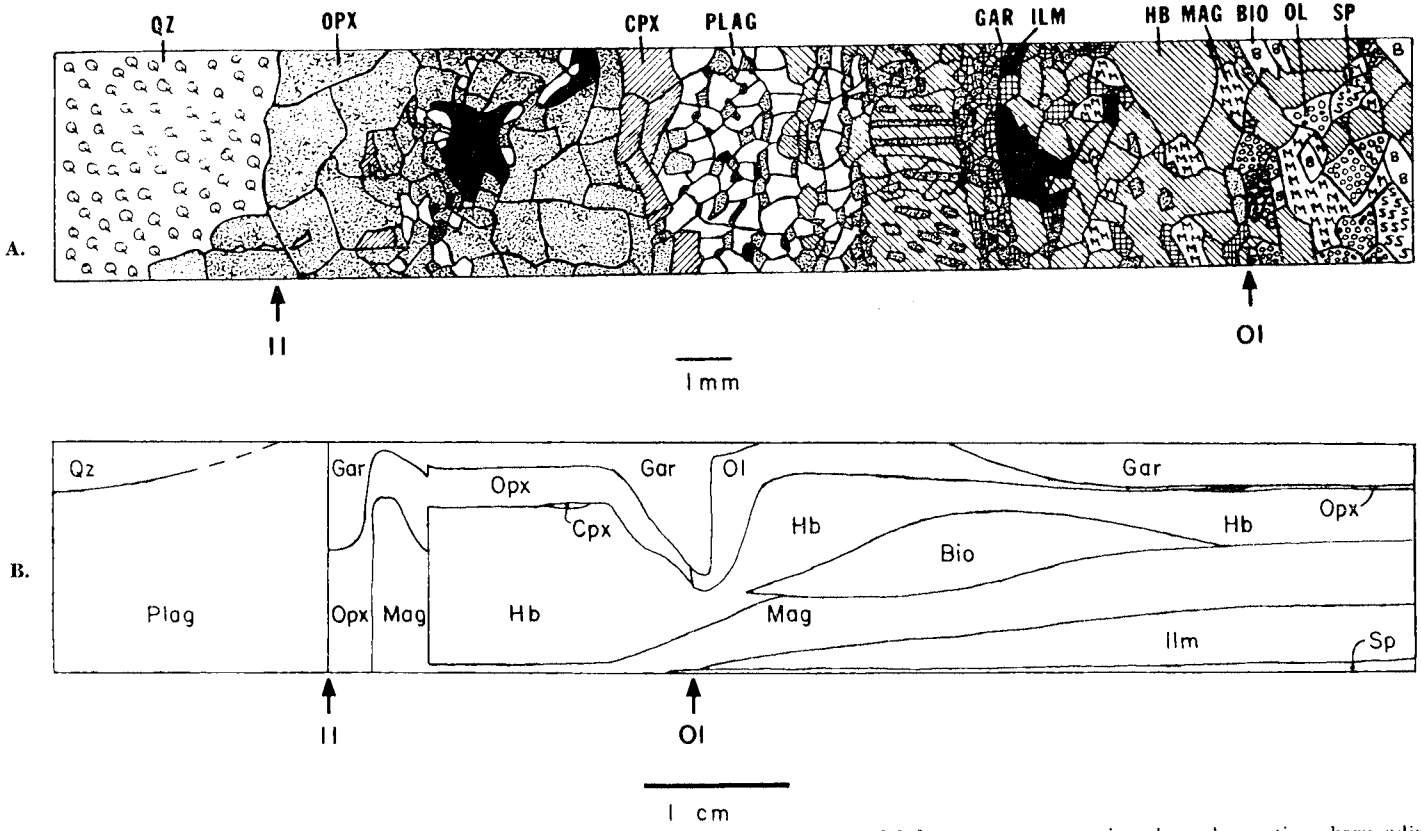

Fig. 1. (A) Schematic line drawing of skarn adjacent to quartz veins. (B) Modal frequency cross section through reaction skarn adjacent to plagioclase quartz dike. Mineral symbols are as follows: Qz, quartz; Plag, plagioclase; Gar, garnet; Opx, orthopyroxene; Mag, magnetite; Hb, hornblende; Cpx, clinopyroxene; Ol, olivine; Bio, biotite; Ilm, ilmenite; Sp, spinel. OI and II indicate the location of the outer and inner interfaces.

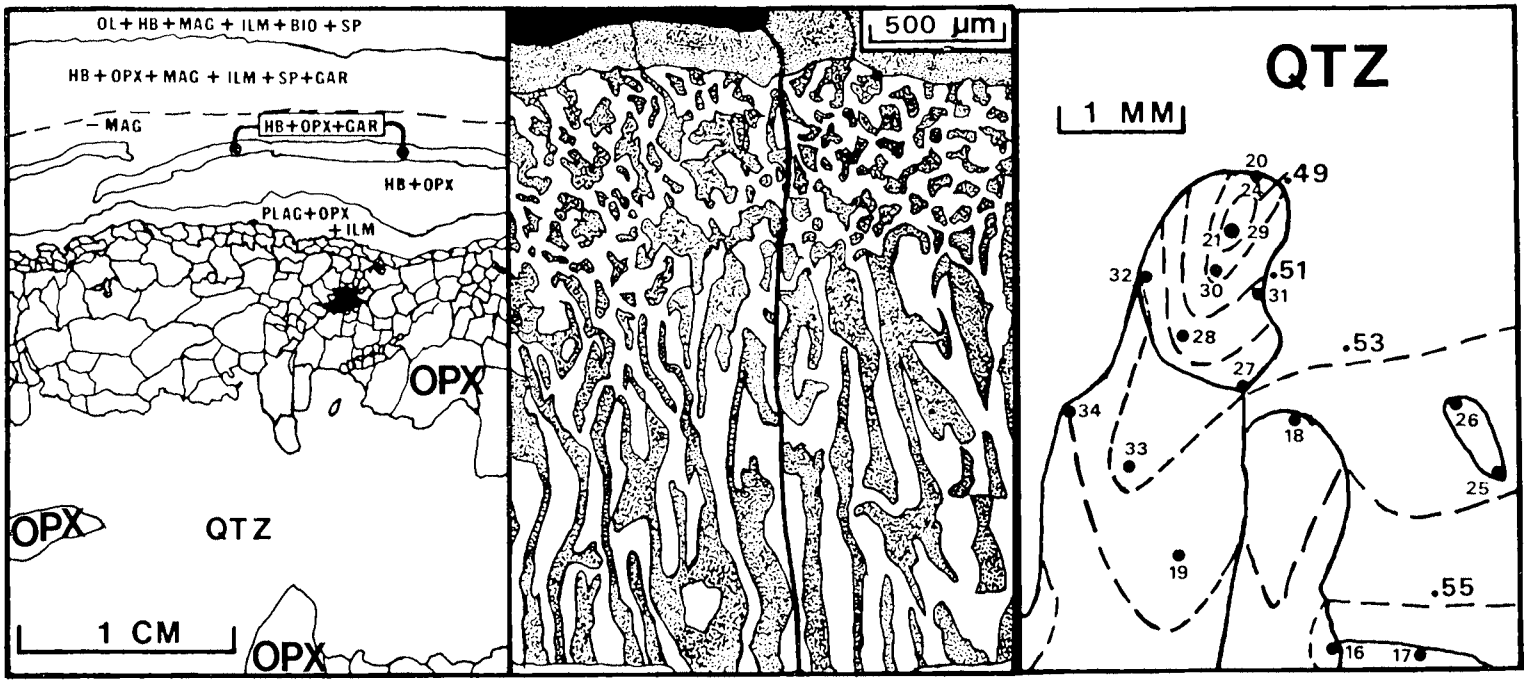

Fig. 2. Line drawings from microphotographs. (A) This figure shows the locations of orthopyroxene inclusions in the quartz vein and the locations of zone boundaries between the almost monomineralic orthopyroxene zone adjacent to the quartz vein and the olivine-bearing rock. The sketch of the orthopyroxene zone adjacent to the vein is partly schematic. Mineral symbols are as follows: Qtz, quartz; Opx, orthopyroxene; Ol, olivine; Ilm, ilmenite; Mag, magnetite; Gar, garnet; Plag, plagioclase; Sp, spinel; Bio, biotite; Hb, hornblende. (B) Orthopyroxene-garnet symplectite adjacent to plagioclase-quartz dike. Mineral symbols are as follows: opaque, magnetite; stipled, orthopyroxene; clear, garnet. Solid line in center of figure delimits different optical orientations of orthopyroxenes. Garnet grain boundaries are not shown. (C) Fe/(Fe + Mg) zoning patterns in orthopyroxene protuberance in quartz vein shown in figures 1A and 3A. Approximate Fe/(Fe + Mg) contours are indicated by dashed lines; dots indicate locations of microprobe analyses given in table 1.

Additional differences between the two skarns are found in the proportions and distributions of Fe-Ti oxide phases to the inner side of the outer interface, in the zonal distribution of garnet, and in the geometry of the inner interface. In both reaction skarns the proportions of Fe-Ti oxides may be used to subdivide them into zones that retain characteristics of the country rock. In the skarn next to the plagioclase-quartz dike, the garnet-orthopyroxene zone to the outer side of the inner interface lacks Fe-Ti oxides (fig. 2B). Magnetite grains with coarse ilmenite lamellae account for more than 90 modal percent of the Fe-Ti oxide assemblage within the remaining zones. In the skarn adjacent to the quartz vein, ilmenite comprises less than 3 modal percent of the zone adjacent to the inner interface. This zone is composed predominantly of relatively coarse-grained orthopyroxene with minor quantities of clinopyroxene, plagioclase, and quartz inclusions. Indeed, the section shown in figures 1A and 2A was chosen for detailed study due to the anamolous presence of ilmenite in it. Ilmenite is common in the remaining zones of the skarn next to the quartz vein, whereas magnetite is restricted to the outer zones of this skarn (see fig. 2). The plagioclase–orthopyroxene–ilmenite zone next to the inner orthopyroxene zone is not always present. These two zones are separated by a zone composed of clinopyroxene (+ orthopyroxene) which is about 0.1 mm wide. Inclusion of quartz are restricted to the inner side of this zone and are rare. The modal ratio ilmenite/magnetite in the outer zones of both skarns is similar to that in the rocks to the outer side of the outer interfaces.

Garnet is present in practically all zones in the skarn adjacent to the plagioclase-quartz dike, whereas, in the section of the reaction skarn adjacent to the quartz vein shown in figures 1A and 2A, garnet mineralization is limited to a zone approx 0.5 cm wide about 1 cm to the outer side of the inner interface. Garnet is most prominently developed in the Fe-Ti oxide-free zone adjacent to the inner interface of the reaction skarn next to the plagioclase-quartz dike (fig. 2B). It averages about 40 percent of this zone, where it is developed as lamellae in orthopyroxene grains and is separated from contact with a discontinuous layer of magnetite grains by an orthopyroxene mantle approx 0.3 mm wide. Grains of this mantle are in optical continuity with the orthopyroxene grains of the orthopyroxene-garnet zone. Most of the domains of optical continuity extend to the inner interface. In contrast to its lamellar habit in the orthopyroxene-garnet zone, garnet is typically developed as equant grains averaging about 0.15 mm in diameter in both reaction skarns. A notable exception is found in garnets that form exceedingly fine ($\leqslant 10$ mμ) rims between grains of spinel and orthopyroxene between 0.5 and 0.7 mm to the inner side of the outer interface adjacent to the quartz vein. In both reaction skarns garnet is invariably in contact with orthopyroxene. Mutual contacts between orthopyroxene and spinel or orthopyroxene, garnet, and magnetite are not observed. Three-phase contacts between olivine, orthopyroxene, and garnet, and, olivine, orthopyroxene, and spinel are present at the outer interfaces of the skarns next to the dike and vein, respectively.

In both orthopyroxene-bearing reaction skarns lamellar hornblende (several millimeters to half a centimeter in diameter) is found to the outer side of the zone of coarse-grained orthopyroxene. In the reaction skarn adjacent to the dike, no zone containing plagioclase separates the coarse-grained hornblende from the zone of coarse-grained orthopyroxene. In the coarse-grained hornblende adjacent to the dike, three types of lamellae and inclusions may be distinguished. These are (1) exsolution lamellae of cummingtonite, (2) discontinuous lamellae of orthopyroxene and, in rare instances, clinopyroxene 0.03 to 0.01 mm in width, and (3) discontinuous composite lamellae which are 0.1 to 0.3 mm in width and contain orthopyroxene and garnet and, in places, clinopyroxene.

In the skarn next to the dike the outer interface has been largely replaced by garnet. In both skarns the zone of metasomatic alteration extends beyond the orthopyroxene-bearing reaction skarn as evidenced by the development of biotite to the outer side of these interfaces. The rocks to the immediate outer side of these interfaces differ from the country rock in the absence of plagioclase and secondary garnet, and, in places, biotite. The habits of garnet and orthopyroxene to the outer side of the biotite-bearing zone adjacent to the dike are quite different from their habits in the orthopyroxene-bearing reaction skarns. Orthopyroxenes in this band are restricted to the cores of nodules or porphyroblasts of garnet and are typically altered to chlorite. No olivine-orthopyroxene contacts are recorded in a zone of spatial overlap of these minerals, near the edge of the biotite-bearing zone. Garnet in this zone occurs in polycrystalline nodules which average about 0.7 mm in diameter and contain inclusions of hornblende.

The form of the inner interface of the orthopyroxene-bearing reaction skarn developed next to the quartz vein differs from the simple slab geometry with sharp replacement fronts explored by Thompson (1959). The interface between the almost monomineralic orthopyroxene zone and the quartz vein contains protuberances such as those shown in figure 2 A and C. The thickness of this zone appears to be correlated with the density of grain boundaries to the outer side of the inner interface. Additional departures from the simple slab geometry are the presence of isolated grains of orthopyroxene in the quartz vein and the local presence of inclusions of quartz within the orthopyroxene zone. In rare instances these inclusions extend from the inner interface to the zone composed of clinopyroxene and orthopyroxene. Perhaps the most striking contrast between the two orthopyroxene-bearing reaction skarns is the volume of coarse grained orthopyroxene produced in the zone to the outer side of the inner interface. The ratio (volume percent orthopyroxene) × (width of inner orthopyroxene zone)/(distance from outer interface) is about 0.7 for the reaction skarn next to the vein. This is more than 10 times that of the reaction skarn adjacent to the dike.

MINERAL CHEMISTRY

Chemical compositions of the mineral phases were obtained with the ARL-EMX automated microprobe in the Department of Geological Sciences of Harvard University. Supplemental data were collected using the eight spectromemeter ARL-SEMQ microprobe in the Department of Geology and Geophysics of the University of California, Berkeley, Calif. Raw data were corrected according to the correction schemes and factors of Bence and Albee (1968) and Albee and Ray (1970). Natural enstatite was used as a

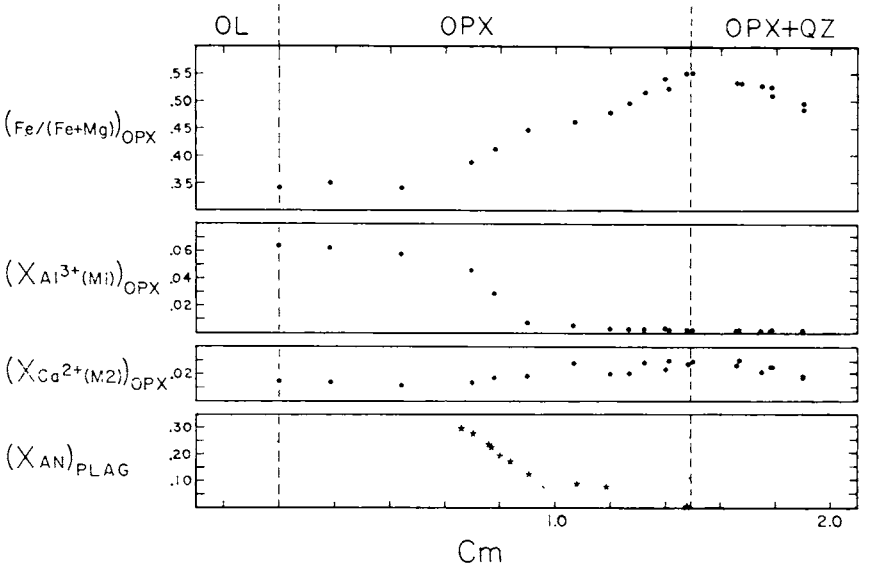

Fig. 3. Compositions variations of the rims of orthopyroxenes and plagioclases across the skarn adjacent to the quartz vein along a segment bounded by the edges of the orthopyroxene protuberance shown in figure 2A and C.

TABLE 1
Microprobe analyses of orthopyroxenes (wt percent oxides)

	V1	V2	V3	V4	V5	V6	V7	V8	V9	V10	V11
CaO	0.40	0.40	0.39	0.33	0.36	0.43	0.48	0.45	0.79	0.48	0.71
FeO	21.17	20.96	21.54	21.30	23.93	23.80	24.95	25.06	27.62	28.05	28.05
MnO	0.17	0.15	0.17	0.18	0.21	0.24	0.24	0.26	0.36	0.25	0.25
MgO	22.56	22.57	22.33	22.95	21.32	21.09	20.38	20.14	18.50	18.21	18.21
TiO_2	0.11	0.11	0.15	0.18	0.09	0.12	0.11	0.09	0.13	0.13	0.13
Al_2O_3	3.03	2.99	2.93	2.81	2.19	2.10	1.52	1.38	0.54	0.40	0.39
SiO_2	51.98	51.65	52.25	51.47	51.82	52.38	52.39	52.39	52.30	52.18	51.46
Total	99.42	98.84	98.96	99.95	99.57	99.60	100.08	99.82	100.24	100.03	99.21
Formula based on 6 oxygens:											
Ca^{2+}	.015	.015	.014	.012	.014	.016	.019	.018	.031	.019	.028
Fe^{2+}	.658	.655	.673	.658	.753	.748	.784	.792	.877	.880	.904
Mn^{2+}	.004	.004	.004	.005	.006	.006	.006	.007	.011	.008	.008
Mg^{2+}	1.250	1.258	1.246	1.263	1.196	1.182	1.141	1.131	1.053	1.079	1.047
Ti^{4+}	.002	.002	.002	.003	.002	.003	.002	.002	.003	.002	.003
Al^{3+}	.132	.131	.128	.121	.096	.092	.067	.061	.023	.018	.017
Si^{4+}	1.932	1.932	1.926	1.932	1.938	1.948	1.968	1.974	1.996	1.989	1.985
Total	3.993	3.997	3.996	3.994	4.006	3.996	3.987	3.985	3.994	3.994	3.992
Fe/(Fe+Mg)	.345	.342	.351	.343	.388	.389	.409	.414	.454	.449	.463
D	0.00	0.00	0.19	0.44	0.69	0.69	0.76	0.78	0.90	0.90	1.07
R/C	R	R	R	R	R	C	C	R	C	R	R
N*	2	2	2	2	2	1	2	2	2	2	2

	V12	V13	V14	V15	V16	V17	V18	V19	V20	V21
CaO	0.50	0.53	0.73	0.59	0.72	0.71	0.66	0.95	0.46	0.46
FeO	29.09	29.49	31.05	32.55	32.87	32.88	32.15	31.59	30.17	29.20
MuO	0.29	0.29	0.30	0.35	0.30	0.30	0.38	0.29	0.19	0.25
MgO	17.58	16.82	17.32	15.41	14.90	15.04	14.90	15.68	16.96	17.88
TiO_2	0.10	0.18	0.09	0.05	0.10	0.11	-	-	-	-
Al_1O_3	0.24	0.33	0.12	0.21	0.20	0.17	0.15	0.27	0.12	0.12
SiO_2	51.40	52.07	51.36	50.80	50.53	51.18	51.20	51.62	52.09	52.20
Total	99.19	99.71	100.06	99.97	99.62	100.39	100.11	100.00	99.98	100.11
Formulas based on 6 oxygens:										
Ca^{2+}	.020	.021	.029	.024	.030	.028	.027	.039	.018	.018
Fe^{2+}	.943	.951	1.008	1.065	1.082	1.073	1.047	1.028	.973	.937
Mu^{2+}	.009	.009	.009	.011	.009	.009	.009	.009	.005	.008
Mg^{2+}	1.016	.967	.943	.898	.875	.875	.910	.887	.975	1.022
Ti^{4+}	.002	.004	.002	.001	.002	.002	-	-	-	-
Al^{3+}	.010	.015	.009	.009	.008	.007	.005	.011	.004	.004
Si^{4+}	1.992	2.008	1.995	1.989	1.991	1.998	1.993	2.009	2.009	2.002
Total	3.992	3.975	3.995	3.997	3.997	3.992	3.996	3.981	3.984	3.991
Fe/(Fe+Mg)	.481	.492	.517	.543	.553	.551	.535	.537	.499	.478
D	1.20	1.27	1.33	1.40	1.48	1.49	SF4	SF4	SF4	SF4
R/C	R	R	R	R	R	R	R	C	R	C
N*	3	3	2	2	2	2	2	1	2	3

TABLE 1 (continued)

	V22	V23	V24	V25	V26	V27	V28	V29	V30	V31	V32
CaO	0.38	0.45	0.47	0.68	0.66	0.55	0.74	0.51	0.49	0.64	0.63
FeO	21.02	20.98	29.58	32.31	31.61	31.60	31.11	29.80	30.32	31.05	31.77
MnO	0.11	0.11	0.17	0.23	0.27	0.22	0.21	0.20	0.19	0.21	0.23
MgO	22.89	22.80	17.56	15.59	15.37	15.71	16.57	17.77	17.20	16.53	15.95
TiO_2	n.a.	n.a.	n.a.	n.a.	n.a.	n.a.	n.a.	n.a.	n.a.	n.a.	n.a.
Al_2O_3	3.04	3.04	0.07	0.14	0.15	0.11	0.14	0.10	0.10	0.09	0.09
SiO_2	52.34	51.40	52.19	50.96	50.97	51.03	51.92	52.44	52.51	51.91	51.11
Total	99.78	98.88	100.04	99.92	99.02	99.21	100.69	100.81	100.81	100.44	99.79
Formulas based on 6 oxygens:											
Ca^{2+}	.015	.017	.019	.023	.028	.022	.029	.020	.019	.026	.026
Fe^{2+}	.651	.654	.952	1.056	1.038	1.036	1.001	.949	.969	1.002	1.037
Mu^{2+}	.003	.003	.004	.007	.008	.007	.005	.005	.005	.005	.007
Mg^{2+}	1.262	1.270	1.007	.908	.901	.919	.951	1.011	.979	.951	.928
Ti^{4+}	n.a.	n.a.	n.a.	n.a.	n.a.	n.a.	n.a.	n.a.	n.a.	n.a.	n.a.
Al^{3+}	.131	.132	.002	.005	.006	.004	.006	.004	.004	.004	.004
Si^{4+}	1.937	1.924	2.006	1.993	2.003	2.003	1.998	2.000	2.008	2.003	1.996
Total	3.999	4.000	3.990	3.997	3.984	3.991	3.990	3.989	3.984	3.991	3.998
Fe/(Fe+Mg)	.340	.337	.486	.538	.535	.530	.513	.484	.497	.513	.528
D	0.0	0.0	SF4	SF4	SF4	SF4	SF4	SF4	SF4	SF4	SF4
R/C	C	R	R	R	R	R	C	C	C	R	R
N*	2	2	2	1	1	2	1	1	1	1	1

	V33	V34	V35	V36	V37	D38	D39	D40	D41	D42	D43	D44	D45	D46	D47	D48	D49	D50
Cao	0.83	0.76	0.74	0.76	0.50	0.29	0.33	0.29	0.30	0.36	0.47	0.40	0.43	0.34	0.46	0.68	0.55	0.69
FeO	31.32	31.95	31.39	29.48	20.81	21.18	21.06	21.47	21.42	21.59	21.98	21.39	21.46	21.65	22.03	24.06	27.31	27.89
MnO	0.23	0.25	0.29	0.25	0.11	0.16	0.15	0.14	0.15	0.17	0.14	0.15	0.23	0.24	0.21	0.22	0.25	0.29
MgO	15.61	15.27	15.94	17.71	22.21	23.03	22.79	22.45	22.68	22.55	22.93	23.50	22.49	23.15	22.44	18.95	18.38	17.65
TiO_2	n.a.	n.a.	n.a.	n.a.	n.a.	0.07	0.13	0.07	0.07	0.05	0.05	0.12	0.04	0.05	0.07	n.a.	n.a.	n.a.
Al_2O_3	0.13	0.12	0.11	0.15	3.16	2.41	2.93	2.54	2.32	2.45	1.98	2.33	2.73	2.21	2.14	2.11	1.88	2.56
SiO_2	51.67	49.58	50.58	51.47	51.28	52.41	52.00	51.86	52.48	52.16	52.66	52.55	51.86	52.30	52.66	52.84	53.68	52.05
Total	99.80	97.83	99.05	00.83	98.06	99.55	99.39	98.82	99.42	99.30	100.21	100.45	99.23	99.93	100.01	100.85	102.03	101.11
Formuals based on 6 oxygens:																		
Ca^{2+}	.034	.031	.031	.031	.020	.011	.013	.011	.011	.014	.018	.015	.016	.013	.017	.026	.021	.027
Fe^{2+}	1.019	1.068	1.032	.952	.655	.657	.654	.671	.666	.672	.679	.658	.669	.671	.683	.814	.846	.878
Mu^{2+}	.006	.008	.009	.008	.003	.004	.004	.003	.004	.004	.003	.004	.006	.006	.006	.006	.007	.009
Mg^{2+}	.905	.910	.934	1.019	1.247	1.274	1.261	1.253	1.257	1.252	1.263	1.290	1.251	1.280	1.240	1.057	1.016	.991
Ti^{4+}	n.a.	n.a.	n.a.	n.a.	b.a.	.001	.003	.001	.001	.001	.001	.003	.001	.001	.001	n.a.	n.a.	n.a.
Al^{3+}	.005	.005	.004	.006	.139	.104	.127	.112	.101	.107	.085	.100	.119	.096	.093	.092	.082	.112
Si^{4+}	2.010	1.093	1.990	1.988	1.931	1.945	1.932	1.942	1.951	1.943	1.948	1.934	1.936	1.939	1.953	1.978	1.989	1.960
Total	3.978	4.005	4.000	4.004	3.994	3.997	3.994	3.993	3.991	3.993	3.998	4.003	3.997	4.006	3.993	3.973	3.962	3.978
Fe/(Fe+Mg)	.529	.540	.525	.483	.344	.340	.342	.349	.346	.350	.350	.338	.348	.344	.355	.435	.455	.470
D	SF4	SF4	1.41	1.38	OOI	0.00	0.18	0.18	0.24	0.35	1.80	2.00	2.24	2.27	2.53	2.64	2.75	2.75
R/C	C	R	R	C	R	R	R	C	R	R	R	R	C	R	R	R	R	C
N*	1	1	1	1	2	2	3	2	2	2	2	2	2	2	2	2	2	2

Notation: V, orthopyroxene from reaction skarn adjacent to vein; D, orthopyroxene from reaction skarns adjacent to dike; n.a., not analyzed; D, distance from outer interface (cm); R/C, rim or core; N*, number of analyses averaged; SF4, see figure 4 for analysis location; OOI, orthopyroxene from outer interface from opposite side of vein.

standard for the elements Mg and Si in orthopyroxene, olivine, garnet, spinel, clinopyroxene, ilmenite, magnetite, hornblende, and biotite. Synthetic hematite, natural rhodonite, natural V_2O_5, synthetic uvarovite, natural ilmenite, natural microcline, and natural albite were used as standards for the elements Fe, Mn, V, Cr, Ti, K, and Na in all minerals in which they were analyzed. Synthetic diopside and anorthite were used as standards for the elements Ca and Al in all but plagioclase feldspar. Natural labradorite was used as the standard for Ca, Al, and Si in plagioclase feldspar. Vanadium-titanium overlap corrections were made following the methods outlined in Snetsinger, Bunch, and Keil (1968).

Pronounced compositional variations perpendicular to the vein are found in orthopyroxene and plagioclase. Figure 3 displays the compositions of the rims of plagioclase and orthopyroxene grains along a traverse approximately perpendicular to the outer interface which includes the prominent orthopyroxene protuberance shown in figure 2A and C. Quartz inclusions are not present near this traverse and are not typical in this zone. Along this traverse the $CaAl_2Si_2O_8$ component in plagioclase varies from 28.9 mole percent in contact with orthopyroxene and hornblende to 0.4 mole percent in contact with quartz. Two patterns of chemical zonation are prominent in the rims of orthopyroxenes between the outer and inner interfaces. $Al^{3+}/3$ oxygens in orthopyroxene exhibit a monotonic decrease from 0.066 at the outer interface to 0.002 adjacent to the inner interface. The Fe/(Fe + Mg) ratio of orthopyroxene is approximately constant (0.34) from the outer interface to the contact of the zone of orthopyroxene and hornblende with the plagioclase-rich zone. To the inner side of this contact surface, it increases progressively to a maximum of 0.55 for orthopyroxenes in contact with quartz. Orthopyroxenes to the inner side of this contact surface become more magnesian toward the core of the vein. Clinopyroxenes display similar composition variations in Al^{3+} as orthopyroxenes with which they are in contact. The composition of clinopyroxene in contact with albite and quartz may be used to define an approximate minimum bound on the $Fe^{3+}/(Fe^{2+} + Fe^{3+})$ ratios of clinopyroxenes in the Westport gabbros. Since these pyroxenes will contain negligible $CaAl_2SiO_6$ component, the sodium remaining after allocations for $CaTiAl_2O_6$ and $NaAlSi_2O_6$ components may be balanced to form $NaFeSi_2O_6$ component. The ratio $Fe^{3+}/(Fe^{3+} + Fe^{2+})$ computed in this manner (0.12) is in excellent agreement with the average value of this ratio computed assuming R_2O_3 stoichiometry and charge balance for 59 clinopyroxenes from the Westport gabbros (0.139 ± 0.078) (Sack, ms).

Both orthopyroxene and clinopyroxene may exhibit radial core to rim compositional variations depending on the size of the grains and their location in the zones. Clinopyroxenes developed as a rim between the mineralogic zones dominated by orthopyroxene and plagioclase exhibit enrichments of Na and Al in cores relative to rims. The relatively fine-grained orthopyroxenes to the outer side of the essentially monomineralic orthopyroxene zone exhibit core to rim composition variations similar to the overall composition variations. For a given distance from the outer interface, rims of orthopyroxene grains adjacent to the quartz vein or within protuberances in it have greater Fe/(Fe + Mg) ratios than cores. In such grains the core to rim increase in Fe/(Fe + Mg) averages

about 0.017 ± 0.008 mm parallel to the outer interface. Within protuberances into the quartz vein contours of constant Fe/(Fe + Mg) are concave toward the center of the vein. Approximate contours of Fe/(Fe + Mg) of the largest protuberance are shown in figure 2C.

In general, orthopyroxenes and plagioclase feldspars in the dike and its reaction skarn do not display nearly as pronounced composition variations as those in the reaction skarn surrounding the quartz vein. The mole fraction of $CaAl_2Si_2O_8$ in plagioclase is in the range 0.14 to 0.23 except in the immediate vicinity of quartz grains. Variations within this range are not correlated with the distance of the plagioclase from the inner interface, nor are core to rim variations in these grains consistent, prominent, or spatially ordered. In the immediate vicinity of quartz grains, however, the An mole fraction of plagioclase drops abruptly to values less than 0.05. Fe/(Fe + Mg) ratios of orthopyroxenes from this reaction skarn are confined to the narrow range 0.34 to 0.36, a range similar to that exhibited by orthopyroxenes from the magnetite-ilmenite bearing zones of the reaction skarn surrounding the quartz vein. However, to the immediate inside of the inner interface, orthopyroxenes along grain boundaries between plagioclase feldspar exhibit iron-enrichment up to an Fe/(Fe + Mg) ratio of 0.47 toward the center of the vein (D48-D50, table 1). Variations in $Al^{3+}/3$ oxygens in these orthopyroxenes are limited to the range 0.064 to 0.042 with highest values found in the cores of orthopyroxenes closest to mutual contacts of garnet and spinel. Core to rim variations in these orthopyroxenes are less than 0.010 $Al^{3+}/3$ oxygens.

Garnets from both reaction skarns exhibit limited ranges of $Ca_3Al_2Si_3O_{12}$ mole fraction (0.12-0.166) and Fe/(Fe + Mg) (0.605-0.665). The $Ca_3Al_2Si_3O_{12}$ mole fraction of garnets in close proximity to spinel and orthopyroxene is identical with that found in this assemblage in orthopyroxene-bearing feldspathic cumberlandites (0.12). In the relatively large garnets developed in the outer garnet-bearing zone of the reaction skarn lacking orthopyroxene-quartz contacts, core to rim increases in Fe/(Fe + Mg) are noted. The range of Fe/(Fe + Mg) in the rims of garnets from either reaction skarn is less than 0.03. Spinels are similar in their chemistry to spinels from the unaltered cumberlandite (compare Sack, ms).

The olivines nearest to the quartz vein are the only olivines from the Westport locality that exhibit pronounced compositional zoning. The average core to rim decrease in Fe/(Fe + Mg) for three olivine grains near the outer interface is 0.015 ± 0.007. The rims of these olivines are among the most magnesian olivines found in the cumberlandite layers. Partitioning of Fe and Mg between olivine, orthopyroxene, spinel, and garnet is like that in the country rocks (compare Sack, 1980b). Partitioning of Fe and Mg between hornblende and biotite and the other phases is also like that of the country rocks. Calculating all iron as FeO, the average compositions of hornblende and biotite are

$$K_{0.28}Na_{0.82}Ca_{1.85}FM_{3.86}Ti_{0.47}Al_{2.58}Si_{5.96}O_{22}(OH,Cl,F)_2$$

and

$$K_{0.94}Na_{0.03}FM_{2.36}Ti_{0.39}Al_{1.33}Si_{2.70}O_{10}(OH,Cl,F)_2$$

TABLE 2

Representative microprobe analyses of garnets and olivines (mole percent oxides)

	VG-1	VG-2	VG-3	DG-1	DG-3	DG-4	DG-5	DG-6	DG-7	DG-9	DG-10	DG-11	DG-12	DG-14	DG-15	VOL-1	VOL-2	VOL-3	VOL-4	VOL-5	VOL-6
CaO	5.12	4.87	4.97	5.34	5.31	5.42	6.04	6.44	4.68	4.94	4.82	4.92	4.78	4.61	4.61	0.06	0.03	0.03	0.03	0.05	0.04
FeO	21.00	20.43	20.31	21.01	20.64	20.85	20.71	21.10	21.14	20.70	21.23	20.18	20.49	20.15	21.01	26.70	28.49	27.78	28.39	28.62	28.53
MnO	0.53	0.54	0.52	0.53	0.60	0.60	0.61	0.64	0.58	0.51	0.50	0.51	0.54	0.53	0.56	0.09	0.12	0.08	0.13	0.08	0.10
MgO	11.63	12.83	12.50	11.27	11.92	11.80	11.06	10.63	12.15	12.16	12.43	13.08	12.51	13.07	12.31	39.84	38.44	38.26	37.92	38.75	37.27
$AlO_{3/2}$	24.73	25.12	25.34	25.48	25.24	25.02	25.01	24.73	25.85	25.85	25.30	25.26	24.58	24.95	25.04	—	n.a.	n.a.	n.a.	n.a.	n.a.
SiO_2	38.39	38.18	38.38	38.12	38.17	38.37	38.25	38.52	37.42	38.11	38.87	38.39	38.55	38.34	39.12	34.35	32.95	32.85	33.14	34.07	33.25
Total	101.40	101.97	102.02	101.75	101.88	102.06	101.68	102.06	101.82	101.72	103.11	101.67	101.82	101.74	102.15	100.14	100.03	99.02	99.61	100.57	99.19
D	0.29	0.38	0.38	2.53	2.27	2.00	1.80	1.29	0.18	0.00	-0.43	-2.25	-2.25	-4.45	-4.45	0.00	-0.02	0.00	-0.01	-0.05	-0.07
R/C	R	C	R	R	R	R	R	R	R	R	R	C	R	C	R	R	C	R	C	R	C
N*	3	2	2	4	2	2	2	1	3	3	3	2	3	3	3	5	2	2	2	2	2

Notation: VG, garnet from reaction skarn adjacent to vein; VOL, olivine from reaction skarn adjacent to vein; DG, garnet from reaction skarn adjacent to dike; n.a., not analyzed; D, distance toward dike or vein from outer interface (cm); R/C, rim or core; N*, number of analyses averaged.

where FM is the sum $Fe^{2+} + Mg^{2+} + Mn^{2+}$. Due to the presence of ilmenite and spinel exsolution lamellae in magnetite, the pre-exsolution composition of these grains was estimated by defocused microbeam analyses using spot sizes around 50 μ in diameter. The resulting estimates of magnetite compositions near the outer interfaces of both reaction skarns are similar to those estimated for magnetites in country rocks containing the olivine-orthopyroxene assemblage (table 3). Semiquantitive analyses of the pre-exsolution compositions of the magnetites near the inner interface of the reaction skarn adjacent to the plagioclase-quartz dike could not be obtained due to the presence of coarse ilmenite lamellae in the magnetites. As shown in table 3, ilmenite exhibits a decrease in calculated Fe_2O_3 mole fraction from the outer interface toward the inner interface of the reaction skarn adjacent to the quartz vein. Cores of these ilmenites are enriched in magnesium.

CHEMICAL POTENTIAL GRADIENTS

The relative magnitudes of the chemical potential differences of FeO, MgO, and SiO_2 in the grain boundary network across the orthopyroxene-bearing zones in samples displaying both orthopyroxene-quartz and orthopyroxene-olivine contacts may be deduced by reference to the simpler system MgO–FeO–SiO_2. For the orthopyroxenes whose rim compositions are displayed in figure 3, the grain boundary composition path may be represented on the MgO–FeO–SiO_2 composition plane shown in figure 4. In this figure this path is represented by a tie-line between olivine and orthopyroxene at the outer interface and tie-lines between quartz and the more iron-rich orthopyroxenes that make up the edge of the most prominent protuberance into the quartz vein. For convenience the outer interface and the point of first appearance of quartz in the grain boundary network will be designated as interfaces (1) and (2) respectively in the ensuing discussion.

If minerals in contact are in local equilibrium (Korzhinskii, 1959; Thompson, 1959), the chemical potentials of the oxide components FeO, MgO, and SiO_2 at these interfaces are defined by the expressions

$$<^1>\mu_{FeO} = <^1>\mu_{Fe_2SiO_4,\ OL} - \tfrac{1}{2}\,<^1>\mu_{Fe_2Si_2O_6,\ OPX} \qquad (1')$$

$$<^2>\mu_{FeO} = \tfrac{1}{2}\,<^2>\mu_{Fe_2Si_2O_6,\ OPX} - <^2>\mu_{SiO_2,QZ} \qquad (1'')$$

$$<^1>\mu_{MgO} = <^1>\mu_{Mg_2SiO_4,\ OL} - \tfrac{1}{2}\,<^1>\mu_{MgSi_2O_6,OPX} \qquad (2')$$

$$<^2>\mu_{MgO} = \tfrac{1}{2}<^2>\mu_{Mg_2Si_2O_6,\ OPX} - <^2>\mu_{SiO_2,\ QZ} \qquad (2'')$$

$$<^1>\mu_{SiO_2} = <^1>\mu_{Fe_2Si_2O_6,\ OPX} - <^1>\mu_{Fe_2SiO_4,\ OL} \qquad (3')$$

$$<^2>\mu_{SiO_2} = <^2>\mu_{SiO_2,QZ} \qquad (3'')$$

where the superscripts $<^1>$ and $<^2>$ refer to interfaces (1) and (2). The differences in chemical potentials of FeO, MgO, and SiO_2 between these interfaces given by subtraction of these relations are

$$\Delta\mu_{FeO} = {}^{<1>}\mu_{Fe_2SiO_4,\ OL} - \tfrac{1}{2}\,{}^{<1>}\mu_{Fe_2Si_2O_6,\ OPX} - \tfrac{1}{2}\,{}^{<2>}\mu_{Fe_2Si_2O_6,\ OPX} + {}^{<2>}\mu_{SiO_2,\ QZ} \quad (1)$$

$$\Delta\mu_{MgO} = {}^{<1>}\mu_{Mg_2SiO_4,\ OL} - \tfrac{1}{2}\,{}^{<1>}\mu_{Mg_2Si_2O_6,\ OPX} - \tfrac{1}{2}\,{}^{<2>}\mu_{Mg_2Si_2O_6,\ OPX} + {}^{<2>}\mu_{SiO_2,\ QZ} \quad (2)$$

$$\Delta\mu_{SiO_2} = {}^{<1>}\mu_{Fe_2Si_2O_6,\ OPX} - {}^{<1>}\mu_{Fe_2SiO_4,\ OL} - {}^{<2>}\mu_{SiO_2,\ QZ} \quad (3)$$

The relative magnitudes of these differences may be deduced by reference to a hypothetical composition path in which the composition of orthopyroxene remains constant between interfaces (1) and (2) (see fig. 4).

Providing that the composition of orthopyroxene picked for the hypothetical path is identical to that of the orthopyroxene at interface (1) in the actual path, the value of $\Delta\mu_{SiO_2}$ across these interfaces will be the

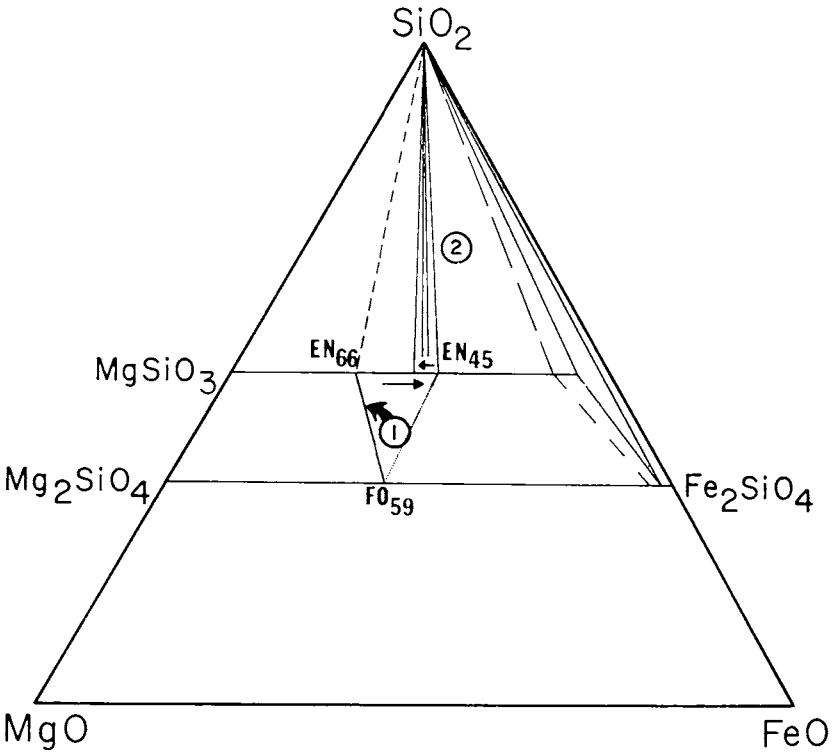

Fig. 4. The composition plane MgO–FeO–SiO_2. Tielines showing Fe-Mg fractionation between olivine and orthopyroxene at interface (1) and the Fe/(Fe + Mg) ratio of orthopyroxene at interface (2) of the reaction skarn adjacent to the quartz vein are indicated by the circled numbers 1 and 2. The finely dotted line indicates the present difference in Fe/(Fe + Mg) ratio between olivines at interface (1) and orthopyroxenes at interface (2). Arrows indicate the direction of change of the Fe/(Fe + Mg) ratio of rims of orthopyroxene grains between interfaces (1) and (2), and, interface (2) and the tip of the orthopyroxene protuberance. Complete triangle and dashed lines representing two sides of a second triangle on the right of the composition plane indicate probable bounds on the Fe/(Fe + Mg) ratios of olivine and orthopyroxene in the stable assemblage olivine–orthopyroxene–quartz at 730°C and 8kb.

same for the hypothetical path and the actual composition path which is characterized by progressively more iron-rich orthopyroxenes toward interface (2). This result may be deduced by inspection of expression (3). In addition, it may be shown that $\Delta\mu_{MgO}$ and $\Delta\mu_{FeO}$ are equal for the hypothetical case of constant orthopyroxene composition between interfaces (1) and (2), because the chemical potentials of $Fe_2Si_2O_6$ and $Mg_2Si_2O_6$ do not vary in this case. For constant values of the chemical potentials of $Fe_2Si_2O_6$ and $Mg_2Si_2O_6$ between interfaces (1) and (2) the difference (2)-(1) may be written as

$$\Delta\mu_{MgO} - \Delta\mu_{FeO} = ({}^{<1>}\mu_{Mg_2SiO_4,\ OL} - {}^{<1>}\mu_{Fe_2SiO_4,\ OL}) - ({}^{<1>}\mu_{Mg_2Si_2O_6,\ OPX} - {}^{<1>}\mu_{Fe_2Si_2O_6,\ OPX}) \quad (4)$$

which requires

$$\Delta\mu_{MgO} = \Delta\mu_{FeO} \quad (5)$$

because the right hand side of (4) is zero if olivine and orthopyroxene are in Mg-Fe exchange equilibrium. It is also apparent that for the hypothetical case of constant orthopyroxene composition between interfaces (1) and (2), the differences $\Delta\mu_{FeO}$, $\Delta\mu_{MgO}$, and $\Delta\mu_{SiO_2}$ are identical in absolute value due to the relation

$$X\mu_{MgO} + (1-X)\mu_{FeO} + \mu_{SiO_2} = \tfrac{1}{2}\,\mu_{(Fe_{(1-X)},\ Mg_X)_2Si_2O_6,\ OPX} \quad (6)$$

Substitution of the equality of $\Delta\mu_{FeO}$ and $\Delta\mu_{MgO}$ into the differences produced by subtraction of two equations of type (6), one for each interface, yields the result

$$\Delta\mu_{FeO} = \Delta\mu_{MgO} = -\Delta\mu_{SiO_2} \quad (7)$$

For the actual diffusion path in which $X_{Fe_2Si_2O_6,\ OPX}$ increases from interface (1) to interface (2), equality (7) is replaced by the inequality

$$\Delta\mu_{FeO} < -\Delta\mu_{SiO_2} < \Delta\mu_{MgO} \quad (8)$$

This inequality is required because the only terms in expressions (1) to (3) that differ for the two paths are ${}^{<2>}\mu_{Fe_2Si_2O_6,\ OPX}$ and ${}^{<2>}\mu_{Mg_2Si_2O_6,\ OPX}$, and these are respectively larger and smaller than for the hypothetical path of constant orthopyroxene composition.

It was noted that beyond interface (2), pyroxenes in contact with quartz become progressively enriched in $Mg_2Si_2O_6$ component toward the core of the quartz vein. The observed increase in the mole fraction of $Mg_2Si_2O_6$ component in orthopyroxene in the presence of quartz requires that the chemical potential of MgO goes through a minimum at interface (2). This may be deduced from the relation

$$\mu_{MgO} = \tfrac{1}{2}\,\mu_{Mg_2Si_2O_6,\ OPX} - \mu_{SiO_2,\ QZ} \quad (9)$$

Consideration of the analogous relation for FeO leads to the conclusion that the chemical potential of FeO decreases from interface (2) toward the center of the quartz vein. Similar constraints do not apply to the zones surrounding the plagioclase-quartz dike due to the absence of orthopyroxene-quartz contacts.

Although the chemical potential paths of oxide components SiO_2, FeO, and MgO may be calculated directly for grain boundary channels between orthopyroxene and quartz beyond interface (2), the chemical potential paths of these components may not be defined directly between interfaces (1) and (2). However, between these interfaces only one of these paths may be regarded as independent due to the relations

$$\mu_{FeO} + \mu_{SiO_2} = \tfrac{1}{2}\,\mu_{Fe_2Si_2O_6,\ OPX} \tag{10}$$

and

$$\mu_{Mg\overline{Fe}} = \mu_{MgO} - \mu_{FeO} = \tfrac{1}{2}\,(\mu_{Mg_2Si_2O_6,\ OPX} - \mu_{Fe_2Si_2O_6,\ OPX}) \tag{11}$$

where the terms on the right hand sides may be calculated from composition data if activity-composition relations and endmember thermochemical data are known and $Mg\overline{Fe}$ is the magnesium-iron exchange component (compare, Thompson and Thompson, 1976). Alternately, given only activity-composition relations, differences of chemical potentials of oxide components MgO, FeO, and SiO_2 between any two points along the diffusion path may be computed from expressions

$$\begin{aligned}&\langle a\rangle\text{-}\langle b\rangle\Delta\mu_{FeO} + \langle a\rangle\text{-}\langle b\rangle\Delta\mu_{SiO_2} = \\ &\tfrac{1}{2}\,RT \ln [\langle a\rangle a_{Fe_2Si_2O_6,\ OPX}/\langle b\rangle a_{Fe_2Si_2O_6,\ OPX}]\end{aligned} \tag{12}$$

and

$$\begin{aligned}&\langle a\rangle\text{-}\langle b\rangle\Delta\mu_{MgO} - \langle a\rangle\text{-}\langle b\rangle\Delta\mu_{FeO} = \\ &\tfrac{1}{2}\,RT \ln [(\langle a\rangle a_{Mg_2Si_2O_6,\ OPX} \cdot \langle b\rangle a_{Fe_2Si_2O_6,\ OPX})/ \\ &\qquad (\langle b\rangle a_{Mg_2Si_2O_6,\ OPX} \cdot \langle a\rangle a_{Fe_2Si_2O_6,\ OPX})]\end{aligned} \tag{13}$$

where $\langle a\rangle$ and $\langle b\rangle$ refer to any two points along the grain boundary channel between interfaces (1) and (2). The corresponding differences defined by the two interfaces may be calculated from the expressions

$$\begin{aligned}\Delta\mu_{FeO} = &+\Delta\mu_1^{\circ} + \tfrac{1}{2}\,RT \ln [(\langle 1\rangle a_{Fe_2SiO_4,\ OL})^2/ \\ &(\langle 1\rangle a_{Fe_2Si_2O_6,\ OPX} \cdot \langle 2\rangle a_{Fe_2Si_2O_6,\ OPX})]\end{aligned} \tag{14}$$

$$\Delta\mu_{SiO_2} = -\Delta\mu_1^{\circ} + RT \ln [\langle 1\rangle a_{Fe_2Si_2O_6,\ OPX}/\langle 1\rangle a_{Fe_2SiO_4,\ OL}] \tag{15}$$

$$\begin{aligned}\Delta\mu_{Mg\overline{Fe}} = &\tfrac{1}{2}\,RT \ln [(\langle 1\rangle a_{Mg_2Si_2O_6,\ OPX} \cdot \langle 2\rangle a_{Fe_2Si_2O_6,\ OPX})/ \\ &(\langle 2\rangle a_{Mg_2Si_2O_6,\ OPX} \cdot \langle 1\rangle a_{Fe_2Si_2O_6,OPX})]\end{aligned} \tag{16}$$

where $\Delta\mu_1^{\circ}$ is the difference $(\mu^{\circ}_{Fe_2SiO_4,\ OL} + \mu^{\circ}_{SiO_2,\ QZ} - \mu^{\circ}_{Fe_2Si_2O_6,\ OPX})$. Most probable values of these differences are shown in figure 5 (see app. 1) along with the chemical potential paths of MgO, FeO, and SiO_2 assuming FeO has a linear chemical potential gradient between interfaces (1) and (2). This assumption may be justified on the basis that the average chemical potential gradient of FeO between interface (1) and (2) is about equal to that defined along the protuberance. Note that the average value of the chemical potential gradient of FeO between interfaces (1) and (2) is approximately equal to that beyond interface (2) where its chemical potential path can be defined directly.

The actual composition path as measured by the composition of orthopyroxenes along the grain boundary network differs by the addition

of pyroxene components containing Al_2O_3, CaO, and TiO_2. For these oxides only the chemical potential path of Al_2O_3 may be defined directly from orthopyroxene composition because Al_2O_3 is an independently variable or actual component (Gibbs, 1928; Thompson, 1959) for all pyroxenes with the exception of the most aluminous pyroxenes which are in contact with garnet. Differences in the chemical potentials of these components cannot be computed with the accuracy of those for FeO, SiO_2, and MgO owing either to the dilute nature of some of the mineral components that contain these oxide components or to the lack of phases containing the mineral components in significant proportions at both interfaces. To summarize calculations in app. 1, chemical potential gradients between interfaces (1) and (2) appear to have been ordered as follows:

$$\left(\frac{d\mu_{CaO}}{dx} \cong 0.03 \pm 0.3\right) < \left(-\frac{d\mu_{FeO}}{dx} \cong 0.47 \pm 0.17\right) < \left(\frac{d\mu_{SiO_2}}{dx} \cong 1.28 \pm 0.15\right) < \left(-\frac{d\mu_{MgO}}{dx} \cong 1.90 \pm 0.20\right) < \left(-\frac{d\mu_{Al_2O_3}}{dx} \geqslant 4.9 \pm 0.2 \text{ kcal/cm}\right) \quad (17)$$

taking directions toward the center of the quartz vein as positive. Except for μ_{FeO}, average one-dimensional gradients of μ_{FeO}, μ_{CaO}, and μ_{MgO} for interface (2) to the tip of the protuberance,

$$-\frac{d\mu_{FeO}}{dx} \cong +0.45 \pm 0.07, -\frac{d\mu_{CaO}}{dx} \cong +2.1 \pm 1.5, \text{ and } \frac{d\mu_{MgO}}{dx} \cong 0.60 \pm 0.05 \text{ kcal/cm}, \quad (18)$$

may be differentiated from the average gradients of these components between interfaces (1) and (2).

In comparison to the reaction skarn adjacent to the vein, the average chemical potential gradient of SiO_2 is considerably smaller across the reaction skarn adjacent to the dike by virtue of the differences in the distances between interface (1) and the first appearance of abundant quartz in the two skarns. Taking into account these differences the average chemical potential gradient of SiO_2 across the latter skarn is calculated to have been 0.5 ± 0.1 kcal/cm. Because the exchange potential μ_{MgFe} of orthopyroxene is approximately constant up to the margin of the dike, chemical potential gradients of FeO and MgO were approximately equal in absolute value but opposite in sign to that of SiO_2 in this reaction skarn. Beyond the margin of the dike the approximate equality of chemical potential gradients of FeO, MgO, and $-SiO_2$ no longer pertains, because isolated grains of orthopyroxene occasionally encountered in this dike within approx 2 mm of its margin exhibit an iron-enrichment trend toward the core of the dike. Thus, in the narrow

zone composed of plagioclase and orthopyroxene at the margin of the dike, the chemical potential gradients of FeO, SiO_2, and MgO were ordered by inequality (8)

$$-\frac{d\mu_{FeO}}{dx} < \frac{d\mu_{SiO_2}}{dx} < -\frac{d\mu_{MgO}}{dx} \tag{19}$$

The average gradient in the chemical potential of $Mg\overline{Fe}$ across this zone, −5 kcal/cm, is the most extreme chemical potential gradient determined for this component in either reaction skarn.

An interesting contrast between the reaction skarns is found in the relative location of the zone adjacent to cumberlandite in which gradients in $\mu_{Al_2O_3}$ first become sizable. In the reaction skarn adjacent to the quartz vein the zone composed of plagioclase, orthopyroxene, and ilmenite exhibits the largest gradient of $\mu_{Al_2O_3}$. Average gradients in $\mu_{Al_2O_3}$ in the remaining zones are negligible by comparison, and the overall gradients

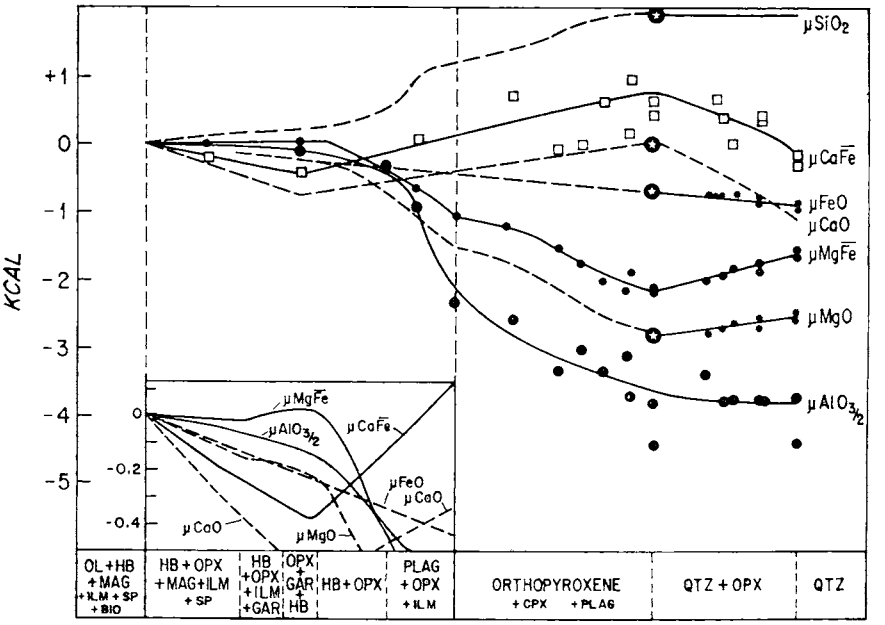

Fig. 5. Calculated oxide and exchange component chemical potential profiles across the skarn next to the quartz vein in kcal/mole. All chemical potentials are assigned the arbitrary value of zero at interface (1). Open squares, small and large filled circles, and asterisks represent values of potentials calculated directly from microprobe data (table 1), the inferred bounds on the three-phase triangle representing phase compositions in the stable assemblage olivine–orthopyroxene–quartz in the compositions plane MgO–FeO–SoO_2 shown in figure 5 and assumptions about the thermodynamic mixing properties of olivine and orthopyroxene detailed in app. I. Solid lines represent potential paths inferred from these calculations; dashed lines represent potential paths for the assumption that the chemical potential gradient of FeO is constant between interfaces (1) and (2). Insert in the lower left corner is a blow up of the profiles shown above it. Zone assemblages are indicated in the strip at the bottom of this figure. Mineral symbols are the same as in figure 2A.

in individual zones are all of the same sign. In the reaction skarn adjacent to the dike, however, the chemical potential of Al_2O_3 follows an oscillatory path from interface (1) to the margin of the dike, before it decreases toward the core of the dike. Due to the absence of orthopyroxene in most of the zone of plagioclase separating the plagioclase-quartz core from the margin of the dike, the chemical potential paths of Al_2O_3 and MgFe cannot be defined over most of this zone. However, the difference of $\mu_{Al_2O_3}$ from the margin of the dike to where quartz appears was likely similar to $\Delta\mu_{Al_2O_3}$ providing the chemical potential of Na_2O was approximately constant due to the relation

$$\tfrac{1}{2}\,\mu_{Al_2O_3} = \mu_{NaAlSi_3O_8,\ PLAG} - 3\mu_{SiO_2} - \tfrac{1}{2}\,\mu_{Na_2O} \qquad (20)$$

and the similar compositions of plagioclase in contact with quartz adjacent to both reaction skarns.

MASS TRANSFER AND MINERAL REACTIONS

Two approaches may be used to evaluate the mass transfer accompanying the formation of the reaction skarns. One of these is to use the compositional and modal data from the individual zones to construct diffusion paths (Darken, 1948, 1949; Thompson, 1975). Quantification of the mass transfer required to form these paths is possible only insofar as the compositions of the original rocks are known and an appropriate reference frame(s) (for example, deGroot and Mazur, 1962; Brady, 1975) can be selected. Alternately it is sometimes possible to evaluate the relative diffusivities of the components selected to describe the diffusion process by examining the profiles of the chemical potentials of these components. Because diffusion of a given component is usually a response to a gradient in the chemical potential of that component, it follows that components that diffuse relatively rapidly will establish smooth variations in their chemical potential profiles. Those that behave in a more inert manner may be characterized by discontinuities in these profiles where the chemical potential gradients of the more inert components are not independent of those of the faster moving components due to the mineral assemblages within the layers of a reaction skarn.

Analysis of the chemical zoning patterns in the reaction skarns is facilitated by the choices of oxide and exchange components to describe the diffusion process. Although these may not always be the species actually diffusing, they are the only components for which chemical potential paths may be unambiguously defined from the mineral assemblages. A further simplifying assumption will be made in the analysis presented here. Following ample petrological precedent (for example, Thompson, 1975; Brady, 1977), it will be assumed that gradients in the chemical potentials of K_2O, Na_2O, H_2O, and H_2 are negligible compared to those of the remaining components due either to their high solubility in an intergranular fluid film or the lack of mineral assemblages defining their chemical potentials at layer contacts or within layers.

Logically the analysis of the mass transfer and mineral reactions involved in the formation of the skarns should begin by developing an analogy between the skarn adjacent to the quartz vein and one composed only of orthopyroxene between masses of olivine and quartz in the simple system MgO–FeO–SiO_2. Although such an analysis yields some insights, it is clear that it is necessary to consider the mineral reactions in more complex chemical systems to explain many features of these skarns. However, in this case it may be demonstrated that these details do not significantly alter the systematics which will be developed from the analysis of the MFS subsystem of the skarn next to the quartz vein. Thus, to streamline the discussion and yet provide a foundation for demonstrating such consistency, the nature and significance of non-MFS reactions are dealt with in app. 2.

As detailed in the previous section, an outstanding feature of the reaction skarn developed next to the quartz vein is the presence of an approximately uniform chemical potential gradient in FeO of -0.47 ± 0.17 kcal/cm between interface (1) and the core of the quartz vein, as opposed to an average chemical potential gradient of -1.90 ± 0.20 kcal/cm for MgO between interfaces (1) and (2). The apparent mobility of FeO, as measured by its ability to level off its chemical potential gradient contrasts sharply with the kinked profile in the chemical potential of MgO in the vicinity of interface (2). As emphasized in the development of expressions (1) to (8), $\Delta\mu_{FeO}$ cannot be changed independently of $\Delta\mu_{MgO}$. For a given olivine composition at interface (1), iron-enrichment of orthopyroxenes toward interface (2) results in an increase in $\Delta\mu_{MgO}$ about equal to the decrease in $\Delta\mu_{FeO}$ relative to the absolute value of $\Delta\mu_{SiO_2}$ which remains unchanged. Mobility of FeO relative to MgO is further emphasized by the absence of core to rim iron-enrichment in olivines near interface (1).

In the skarn adjacent to the quartz vein the pattern of intracrystalline chemical zonation in orthopyroxene protuberances and the essentially monomineralic orthopyroxene zone emphasize the relative importance of grain-boundary as opposed to volume diffusion in maintaining the apparent mobility of FeO during the metamorphism of these zones. If the generation of the chemical patterns of this reaction skarn is ascribed to conditions of essentially constant temperature and pressure, then the pattern of chemical zonation in orthopyroxenes near interface (2) (iron-enrichment along grain boundaries relative to cores) records the successive diminution of the chemical potential differences of FeO across the skarn during its growth. Based on analogy with an orthopyroxene skarn in the system MgO–FeO–SiO_2, however, it is difficult to ascribe the development of this zoning pattern to the establishment of a steady state at a given temperature and pressure because this would lead to Fe-Mg zoning opposite to that observed.

In a steady state (Fisher, 1973; Joesten, 1977) the values of the chemical potential differences of MgO and FeO across the skarn are determined by the compositions of olivine and orthopyroxene at interfaces (1) and (2)

and the fluxes of FeO and MgO generated by the reaction at interface (1), $^{<1>}J_{FeO}$ and $^{<1>}J_{MgO}$. In attaining a steady state the ratio $\Delta\mu_{FeO}/\Delta\mu_{MgO}$ adjusts such that the flux ratio $^{<1>}J_{FeO}/^{<1>}J_{MgO}$ from interface (1) is that required to produce orthopyroxene of constant composition at interface (2), after it is altered by precipitation and exchange reactions across the skarn. Consider, for example, the growth of a planar diffusion zone of orthopyroxene between olivine and quartz rocks in the system MgO–FeO–SiO_2. If we assume that the composition of olivine remains constant at interface (1) and choose FeO, MgO, and SiO_2 as components to describe the diffusion process, then the reaction at interface (1) may be written as

$$\begin{aligned} {}^{<1>}\nu_{SiO_2} + (Mg_x, Fe_{(1-x)})_2SiO_4 = (1 + {}^{<1>}\nu_{SiO_2})/2\ (Mg_y, Fe_{(1-y)})_2Si_2O_6 \\ + 2\ [x - y\ (1 + {}^{<1>}\nu_{SiO_2})/2]\ MgO \\ + 2\ [(1-x) - (1-y)\ (1 + {}^{<1>}\nu_{SiO_2})/2]\ FeO \end{aligned} \tag{21}$$

where $^{<1>}\nu_{SiO_2}$ is the reaction coefficient of SiO_2 at interface (1) which may vary between 0 and 1. The composition of orthopyroxene at interface (1) is determined by the equilibrium distribution coefficient for Fe-Mg exchange between olivine and orthopyroxene, $K_D = y(1-x)/(x(1-y)) \cong 1.34$ for $X_{Mg_2SiO_4, OL} = 0.6$. It is evident from expression (21) that the flux ratio $^{<1>}J_{FeO}/^{<1>}J_{MgO}$ is a function of both the distribution coefficient for Fe-Mg exchange among olivine and orthopyroxene and the rate of transfer of SiO_2 to interface (1) relative to that of (FeO + MgO), FMO, to interface (2). Because orthopyroxene is more magnesian than the olivine with which it is in Fe-Mg exchange equilibrium, at least for the range of olivine compositions observed here (compare Sack, 1980a), the flux ratio $^{<1>}J_{FeO}/^{<1>}J_{MgO}$ generated from this reaction will be greater than the Fe/Mg ratio of olivine at interface (1). For an olivine with $X_{Mg_2SiO_4, OL}$ of 0.6 the value of the ratio $^{<1>}J_{FeO}/^{<1>}J_{MgO}$ generated from reaction (21) would be between 0.88 and 1.53 for values of $^{<1>}\nu_{SiO_2}$ between 0.0 and 0.5. During the growth of the skarn the reaction at interface (1) would lead to iron enrichment of orthopyroxenes toward interface (2). This will diminish the difference of $|\Delta\mu_{FeO}|$ and augment the difference $|\Delta\mu_{MgO}|$ until the average fluxes of FeO and MgO across the reaction skarn.

$$\bar{J}_{FeO} = -\bar{L}_{FeO}\ (\Delta\mu_{FeO}/\Delta x) \tag{22}$$

and

$$\bar{J}_{MgO} = -\bar{L}_{MgO}\ (\Delta\mu_{MgO}/\Delta x) \tag{23}$$

are similar to the coefficients of these components in the reaction at interface (1).[1] Assuming that a steady state was established in this manner, the calculated gradients and observed compositions of olivine and orthopyroxene suggest that the ratio $\bar{L}_{FeO}/\bar{L}_{MgO}$ was about 5 in the skarn adjacent to the quartz vein.

[1] Here the L_i coefficients represent the products $(C_iD_i)/(RT)$, C_i and D_i are the intergranular concentrations, and diffusion coefficients of components i, L_{FeO}, and L_{MgO} are the average values of compositionally dependent phenomenological diffusion coefficients for FeO and MgO ($L_{FeO} > L_{MgO}$), Δx is the thickness of the skarn, and the possibility of diffusion of a given component in response to a gradient in the chemical potential of another component is neglected.

As mentioned above, however, it is unlikely that the Fe-Mg zoning patterns in orthopyroxenes near interface (2) are consistent with the establishment of a steady state at a given temperature and pressure, at least based on analogy with an orthopyroxene skarn in the system MgO–FeO–SiO_2. If a steady state were established in such a skarn, orthopyroxenes near interface (2) would be zoned in Fe-Mg. However, they would have more magnesian rims than cores, because the composition of orthopyroxene at interface (2) would remain constant with growth of the skarn. As the layer of orthopyroxene widens, orthopyroxenes lying between interface (1) and the initial contact would be more magnesian than required by local equilibrium between orthopyroxene and the exchange medium whereas orthopyroxenes lying between the initial boundary and interface (2) would be less magnesian than so required. Zoning would result from continued internal precipitation of orthopyroxene or by exchange with the intergranular medium. This would result in orthopyroxenes in the vicinity of interface (2) having iron-rich cores and magnesium-rich rims, the opposite of that observed. Alternately, the progressive iron-enrichment of orthopyroxenes near interface (2) may be due to changes in the temperature and pressure of metamorphism. This possibility will be considered more fully in the ensuing discussion.[2]

In contrast to FeO and MgO, for which relative diffusivities may be deduced from the grain-boundary zoning patterns, the approximate diffusivity of SiO_2 relative to FeO + MgO, FMO, may be deduced by defining the location of the initial reaction interface. Two lines of evidence suggest that in the skarn next to the vein the initial reaction interface was between the zone composed of plagioclase, orthopyroxene, and ilmenite and the essentially monomineralic orthopyroxene zone. First, assuming Al_2O_3 and TiO_2 are among the most inert components, the concentrations of these components indicate that the initial contact was here because orthopyroxenes in the inner orthopyroxene zone have negligible concentrations of Al_2O_3 relative to those in outer zones and Fe-Ti oxides are normally present only in these outer zones and in cumberlandite. Because Al_2O_3 is an independent component of orthopyroxene, the change in Al_2O_3 concentration in orthopyroxenes in the plagioclase–orthopyroxene–

[2] The reader will note that the possibility of zoning of olivine near interface (1) was not considered in developing a steady state analogy for the reaction skarn in the system MgO–FeO–SiO_2. Should zoning develop in the olivines, it would not significantly affect the systematics presented here. Indeed it is possible that during the initial reaction the quantities of FeO and MgO that expression (21) predicts would be generated at interface (1) would define a value of $(\mu_{FeO} - \mu_{MgO})$ in the intergranular medium differing from that defined by the initial olivine composition. If this were the case, olivines near this interface would become more iron-rich or magnesium-rich depending on the sign of the inequality. This enrichment would continue until a balance was achieved whereby the ratio FeO/MgO produced by the reaction at interface (1) was balanced by disposal by diffusion into the skarn and by interdiffusion into crystals along this interface and along grain-boundary channels in the olivine rock in response to gradients in $(\mu_{FeO} - \mu_{MgO})$ generated by the change in olivine composition at interface (1). Whether zoning develops depends on the rate of supply of MgO and FeO from the reaction at this interface relative to that required to maintain or adjust the composition gradient along grain boundary channels within the skarn such that $|\Delta\mu_{FeO}| < |\Delta\mu_{MgO}|$.

ilmenite zone defines a steep slope for ($d\mu_{Al_2O_3}/dr$) across this zone; this is in contrast to the relatively negligible slopes of ($d\mu_{Al_2O_3}/dr$) in the remaining orthopyroxene-bearing zones between the inner and outer interfaces (see fig. 5). Sporadic quartz inclusions in the inner orthopyroxene zone provide a second line of evidence that the initial reaction interface was between the zone composed of plagioclase, orthopyroxene, and ilmenite and the inner orthopyroxene zone. However, this interface may not be a strict marker of the boundary between the original lithologies owing to the local occurrence of ilmenite in the inner orthopyroxene zone. Such fragments may have been generated during the introduction of the quartz vein.

The considerations given above suggest that, at least for the reaction skarn adjacent to the quartz vein, the flux of SiO_2 across the initial reaction interface was small compared to those of FeO and MgO. This may be illustrated by considering expression (21) for an orthopyroxene skarn between olivine and quartz rocks. If $^{<1>}\nu_{SiO_2}$ is zero in this expression, then the number of moles of orthopyroxene on each side of the initial reaction interface will be about equal because for each mole of orthopyroxene formed at interface (1), two moles of FMO will be generated for diffusion across the skarn and reaction with quartz at interface (2). With increasing $^{<1>}\nu_{SiO_2}$ the proportion of the orthopyroxene skarn growing into the quartz vein would decrease until, in the limit that $^{<1>}\nu_{SiO_2}$ is one, orthopyroxene would form only by the reaction at interface (1). Although the actual case represented by the reaction skarn adjacent to the quartz vein must be somewhere between these extremes, it appears that it was very close to the former case because the volume of the skarn between interface (1) and the initial reaction interface is about equal to the volume of orthopyroxene between this interface and the center of the quartz vein (see fig. 2A). This comparison is not strictly correct, however, because olivine does not comprise all of the cumberlandite, and, as detailed in app. 2, both magnetite-breakdown and biotite-forming reactions contributed to the flux of FMO across the initial reaction interface. However, because these differences approximately counterbalance each other, we may conclude that for the reaction skarn adjacent to the quartz vein, the diffusion of SiO_2 across the initial reaction was small compared to counterdiffusion of MgO and FeO across it.

Although the flux of SiO_2 across the reaction skarn adjacent to the quartz vein was small compared to MgO and FeO, at least local diffusion of SiO_2 across the outer margin of the plagioclase-quartz dike was required to produce the inner zone of the adjacent skarn. This is demonstrated by the absence of quartz within the immediate outer margin of the dike next to the inner garnet-orthopyroxene zone of its associated skarn. Further, the two reaction skarns provide an interesting contrast in the quantities of (FeO + MgO) supplied for the growth of the orthopyroxene or orthopyroxene-garnet zones developed at the expense of the introduced material relative to the overall thicknesses of the orthopyroxene-bearing zones. In the reaction skarn adjacent to the plagioclase-quartz dike, the

"initial contact" is also marked by Fe-Ti oxides. Proceeding from the dike to interface (1), the initial contact surface or zone is marked by magnetite. The composite zone consisting of orthopyroxene-garnet intergrowths and the orthopyroxene mantle separating the garnet in these intergrowths from contact with magnetite represents only approximately one-eighth of the total volume of the orthopyroxene-bearing skarn adjacent to the dike, whereas the orthopyroxene zone developed by replacement of the quartz vein comprises about 45 volume percent of the other skarn. Taking into account the density of FMO in these zones, it is estimated that for the reaction skarn adjacent to the plagioclase-quartz dike the ratio ($J_{FMO}{}^{IC}/\Delta x$) (flux of FMO/cm^2 past the initial interface/total thickness of orthopyroxene-bearing skarn) is about 0.23 that for the reaction skarn adjacent to the quartz vein. The smaller ratio ($J_{FMO}{}^{IC}/\Delta x$) for the orthopyroxene-bearing skarn adjacent to the dike is readily understood in light of the present absence of the orthopyroxene-quartz assemblage at the contact between this skarn and the dike.

DISCUSSION

Several origins may be suggested for the patterns of intracrystalline zoning of Fe/(Fe + Mg) of orthopyroxenes and olivines within the reaction skarn adjacent to the quartz vein. The observed pattern of intracrystalline zonation is equivalent to clockwise rotation of the dotted line in figure 4 or counterclockwise rotation of the Fe/(Fe + Mg) profile as shown in figure 6. As mentioned above, for a skarn within the MFS sys-

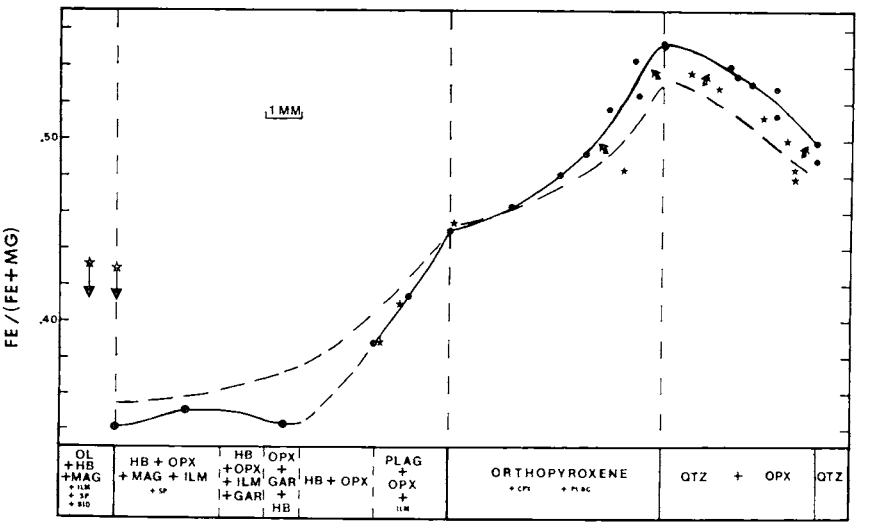

Fig. 6. Fe/(Fe + Mg) profile for olivines and orthopyroxenes across the reaction skarn adjacent to the quartz vein. Filled circles and tips of arrows indicate the present rim compositions of orthopyroxenes and olivines. Open and filled stars represent the Fe/(Fe + Mg) ratios of cores of olivine and orthopyroxene grains. The present grain boundary path of Fe/(Fe + Mg) ratios of orthopyroxenes is indicated by the solid curve; a possible earlier path is indicated by the dashed curve. Zone assemblages are indicated in the strip at the bottom of this figure. Mineral symbols are the same as in figure 2A.

tem, it is difficult to reconcile the pattern of Fe-Mg zoning of orthopyroxenes near interface (2) with an origin by isothermal diffusion alone. For such a skarn this pattern may be readily explained by changes in temperature and pressure. Possible bounds on such changes may be developed from analysis of the thermodynamic equations for the MFS skarn. These bounds are consistent with those derived from (1) garnet-bearing corona structures within the surrounding rocks (Sack, 1977, 1980b), (2) the chemical zoning of orthopyroxenes in the dike next to the garnet-orthopyroxene zone of the adjacent skarn, and (3) the distribution of garnet within both skarns.

The system of thermodynamic equations which relate changes in temperature, pressure, and $\Delta\mu_{FeO}$ for a MFS reaction skarn is given in table 4. This system consists of equations of three types: (1) Gibbs-Duhem equations for mineral phases at layer contacts, (2) stoichiometric equations needed to eliminate linearly dependent components, and (3) relations between chemical potential and independent mole fraction variables.[3] For the limiting assumption that $d(\Delta\mu_{FeO})/dt \sim 0$, bounds on possible temperature or pressure variations consistent with the Fe-Mg zoning of minerals near interfaces (1) and (2) may be approximated through the relations

$$\Delta T = \left(\frac{\partial T}{\partial(^{<1>}X_{1,\,OL})}\right)_{P,\,^{<2>}X_{3,\,OPX},\,\Delta\mu_{FeO}} (^{<1>}X_{1,\,OL} - ^{<c>}X_{1,\,OL}) + \left(\frac{\partial T}{\partial(^{<2>}X_{3,\,OPX})}\right)_{P,\,^{<1>}X_{1,\,OL},\,\Delta\mu_{FeO}} (^{<2>}X_{3,\,OPX} - ^{<c>}X_{3,\,OPX}) \quad (24)$$

$$\Delta P = \left(\frac{\partial P}{\partial(^{<1>}X_{1,\,OL})}\right)_{T,\,^{<2>}X_{3,\,OPX},\,\Delta\mu_{FeO}} (^{<1>}X_{1,\,OL} - ^{<c>}X_{1,\,OL}) + \left(\frac{\partial P}{\partial(^{<2>}X_{3,\,OPX})}\right)_{T,\,^{<1>}X_{1,\,OL},\,\Delta\mu_{FeO}} (^{<2>}X_{3,\,OPX} - ^{<c>}X_{3,\,OPX}) \quad (25)$$

where $^{<c>}X_{1,\,OL}$ and $^{<c>}X_{3,\,OPX}$ are the mole fractions of Mg_2SiO_4 and $Mg_2Si_2O_6$ in the cores of olivines and orthopyroxenes near interfaces (1) and (2) respectively, and the derivatives $(\partial P/\partial X_i)_{T,X_j}$ and $(\partial T/\partial X_i)_{P,X_j}$ may be obtained from solution of the system of equations in table 4.

Solution of this system of equations for the condition $\Delta T = 0$, for example, gives the result

$$\Delta P = \frac{^{<1>}\overline{G}_{11,\,OL}\,(^{<1>}X_{1,\,OL} - ^{<1>}X_{3,\,OPX}/2)}{\Delta\bar{V}^*}(^{<1>}X_{1,\,OL} - ^{<c>}X_{1,\,OL}) - \frac{^{<2>}\overline{G}_{33,\,OPX}\,(^{<2>}X_{3,\,OPX}/2)}{\Delta\bar{V}^*}(^{<2>}X_{3,\,OPX} - ^{<c>}X_{3,\,OPX}) \quad (26)$$

[3] Development of relations with the form of the third set of equations is outlined by Thompson and Thompson (1976).

TABLE 4

Thermodynamic equations

	dT	dP	$^{1}\mathrm{d}(\mu_1-\mu_2)$	$^{1}\mathrm{d}\mu_2$	$^{1}\mathrm{d}(\mu_3-\mu_4)$	$^{1}\mathrm{d}\mu_4$	$^{2}\mathrm{d}(\mu_3-\mu_4)$	$^{2}\mathrm{d}\mu_4$	$^{2}\mathrm{d}\mu_5$	$^{1}\mathrm{d}X_{1,\,OL}$	$^{2}\mathrm{d}X_{3,\,OPX}$	$\mathrm{d}(\Delta\mu_{FeO})$
(1)	$0=+{}^{1}\bar{S}_{OL}$	$-{}^{1}\bar{V}_{OL}$	$+{}^{1}X_{1,\,OL}$	$+1$	0	0	0	0	0	0	0	0
(2)	$0=+{}^{1}\bar{S}_{OPX}$	$-{}^{1}\bar{V}_{OPX}$	0	0	$+{}^{1}X_{3,\,OPX}+1$	0	0	0	0	0	0	0
(3)	$0=+{}^{2}\bar{S}_{OPX}$	$-{}^{2}\bar{V}_{OPX}$	0	0	0	0	$+{}^{2}X_{3,\,OPX}$	$+1$	0	0	0	0
(4)	$0=+{}^{2}\bar{S}_{QZ}$	$-{}^{2}\bar{V}_{QZ}$	0	0	0	0	0	0	$+1$	0	0	0
(5)	$0=$ 0	0	-1	0	$+1$	0	0	0	0	0	0	0
(6)	$0=$ 0	0	0	-1	0	$+\frac{1}{2}$	0	$+\frac{1}{2}$	-1	0	0	-1
(7)	$0=-({}^{1}\bar{S}_{1,\,OL}-{}^{1}\bar{S}_{2,\,OL})+$	$({}^{1}\bar{V}_{1,\,OL}-{}^{1}\bar{V}_{2,\,OL})$	-1	0	0	0	0	0	0	${}^{1}\overline{G}_{11,\,OL}$	0	0
(8)	$0=-({}^{2}\bar{S}_{3,\,OPX}-{}^{2}\bar{S}_{4,\,OPX})+$	$({}^{2}\bar{V}_{3,\,OPX}-{}^{2}\bar{V}_{4,\,OPX})$	0	0	0	0	-1	0	0	0	${}^{2}G_{33,\,OPX}$	0

Notation: ${}^{1}X_{1,\,OL}$, mole fraction Mg_2SiO_4 is olivine at interface (1); ${}^{1}X_{3,\,OPX}$, mole fraction of $Mg_2Si_2O_6$ in orthopyroxene at interface (1); ${}^{2}X_{3,\,OPX}$, mole fraction of $Mg_2Si_2O_6$ in orthopyroxene at interface (2); ${}^{1}\bar{S}_{OL}$, molar entropy of olivine at interface (1); ${}^{1}\bar{V}_{OL}$, molar volume of olivine at interface (1); ${}^{1}\bar{S}_{1,\,OL}$, partial molar entropy of Mg_2SiO_4 in olivine at interface (1); ${}^{1}\bar{V}_{1,\,OL}$, partial molar volume of Mg_2SiO_4 in olivine at interface (1); ${}^{2}\overline{G}_{33,\,OPX}$, $(\partial^2({}^{2}\overline{G}_{OPX})/\partial({}^{2}X_3)^2)_{P,T}$. Eqs (1) to (4) are Gibbs-Duhem equations; eqs (5) and (6) are stoichiometric equations needed to eliminate linearly dependent components; eqs (7) and (8) are relations between chemical potential and independent mole fraction variables.

where

$$\Delta\bar{V}^* = [{}^{<1>}\bar{V}_{OL} + {}^{<2>}\bar{V}_{QZ} - ({}^{<1>}\bar{V}_{OPX} + {}^{<2>}\bar{V}_{OPX})/2] + ({}^{<2>}\bar{V}_{3,\,OPX} - {}^{<2>}\bar{V}_{4,\,OPX})({}^{<2>}X_{3,\,OPX}/2) - ({}^{<1>}\bar{V}_{1,\,OL} - {}^{<1>}\bar{V}_{2,\,OL})({}^{<1>}X_{1,\,OL} - {}^{<1>}X_{3,\,OPX}/2) \quad (27)$$

Assuming ideal mixing and using the molar volume data given in Robie, Bethke, and Beardsley (1967) a value of $\Delta P \cong 1.5$ kb is obtained for the change in interface compositions shown in figure 6. An equivalent expression for ΔT may be written, but, due to uncertainties in entropy terms, a more approximate method will be pursued instead. For the assumptions that $\Delta Cp = 0$, $dP = 0$, and that olivine and orthopyroxene are ideal with respect to thermodynamic mixing properties, we may write relation (14) for two temperatures T_2, the temperature of local metamorphic equilibration, and $T_1 = T_2 - \Delta T$

$$(\Delta\mu_{FeO})_{T_2} = (\Delta\mu_1^o)_{T_2,\,P} + RT_2 \ln IIX_i^r \quad (14')$$

$$(\Delta\mu_{FeO})_{T_2-\Delta T} = (\Delta\mu_1^o)_{T_2,\,P} + \Delta T\Delta\bar{S}_1^o + RT_2 \ln IIX_i^c - R\Delta T \ln IIX_i^c \quad (14'')$$

where IIX_i^r and IIX_i^c are the composition products for interfaces (1) and (2) at present and at T_1 (for example, $IIX_i^r = ({}^{<1>}X_{2,\,OL})^2/({}^{<1>}X_{4,\,OPX}\,{}^{<2>}X_{4,\,OPX})$). Subtracting these relations, the alternate result

$$\Delta T = \left(\frac{[(\Delta\mu_{FeO})_{T_2} - (\Delta\mu_{FeO})_{T_2-\Delta T}] + RT_2 \ln (IIX_i^c/IIX_i^r)}{R \ln IIX_i^c - \Delta\bar{S}_1^o}\right) \quad (28)$$

is obtained. Continuing with the assumption that $d(\Delta\mu_{FeO})/dt = 0$, using the value of $\Delta\bar{S}_1^o$ estimated from the pressure-temperature brackets for the FS endmember reaction of Bohlen, Boettcher, and Essene (1978) combined with volume data via the Claperon equation, and assuming that Fe-Mg fractionation between olivine and orthopyroxene is temperature insensitive for olivines with Fe/(Fe + Mg) around 0.4 (Sack, 1980a), a value of $\Delta T = T_2 - T_1 = -130 \pm 30°$ would be consistent with the change in interface compositions shown in figure 6. For a hypothesis of retrograde cooling, an assumption that $(\Delta\mu_{MgO}/\Delta\mu_{FeO})_{T_1} < (\Delta\mu_{MgO}/\Delta\mu_{FeO})_{T_2}$ ($T_1 > T_2$) is probably more reasonable considering the exponential dependence of diffusivity on temperature. This assumption would suggest that the estimate $T_2 - T_1 = \Delta T = -130 \pm 30°$ is a reasonable minimum bound for the composition changes given in figure 6 because the sum $(\Delta\mu_{FeO} + \Delta\mu_{MgO})$ increases with decreasing temperature.

Although the bounds suggested above must be considered qualitative, they illustrate that the zoning observed in olivines and orthopyroxenes near interfaces (1) and (2) could have resulted from retrograde cooling or increased pressure, and, they are in qualitative agreement with those based on other considerations (see app. 2). As emphasized in footnote 2 and app. 2, however, not all of the zoning in the olivines near interface (1) may be due to such an origin. However, this observation does not

necessarily alter the nature of the conclusions reached. In fact it is likely that due to intracrystalline diffusion, the total changes in compositions of olivines and orthopyroxenes at interfaces (1) and (2) may have been greater than those suggested in figure 6. Indeed, the compositions of orthopyroxenes within the tip of the most prominent orthopyroxene protuberance, Fe/(Fe + Mg) ~ 0.48, and olivines in unaltered cumberlandite (olivine–magnetite–ilmenite rock) of the country rock, Fe/(Fe + Mg) ~ 0.045, suggest that this may have been the case. Given that Fe-Mg inter-

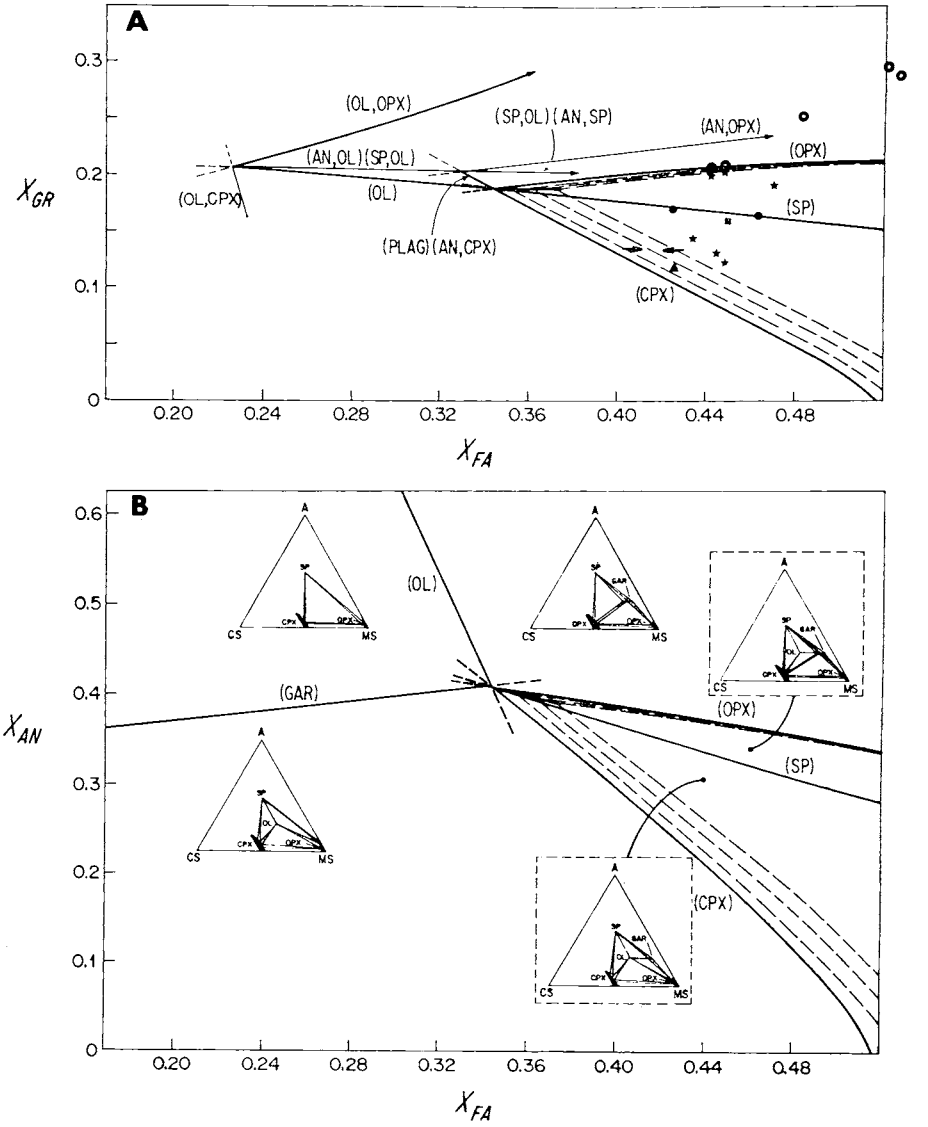

diffusion coefficients of olivines are several orders of magnitude greater than those of orthopyroxenes (for example Buening and Buseck, 1973; Heubner, Ross, and Hickling, 1975; Virgo and Hafner, 1969), it would be anticipated that a larger proportion of the total composition changes might be recorded by orthopyroxenes. However, greater composition changes at interfaces (1) and (2) than given in figure 7 do not necessarily imply that the changes in metamorphic conditions were greater than the bounds suggested above, at least for the retrograde model. For this model, although the composition changes would suggest the terms in the numerator of (28) were different than those suggested above, these differences would be of opposite sign and similar magnitude, and $|\Delta\bar{S}_1^o| > |R \ln \Pi X_i^e|$.

Regardless of the pressure-temperature path(s) responsible for the metamorphism of these reaction skarns, they illustrate several aspects of the mechanisms of metamorphic reactions of apparently dry mafic rocks at high grades of metamorphism.[4] (1) They suggest that grain-boundary

← Fig. 7. Relationships between compositions of olivine, plagioclase, and garnet in low variance assemblages in country rocks at 730 ± 50°C and 8 ± 1 kb from Sack (1980b). (A) Calculated diagram showing the mole fraction of $Ca_3Al_2Si_3O_{12}$ in garnet (X_{GR}) as a function of MgFe exchange potential as measured by olivine composition for bi- and trivariant subassemblages of the six-phase assemblage olivine–orthopyroxene–clinopyroxene–spinel–garnet–plagioclase in the systems FMAS, CFMAS, and NCFMAS and tri- and quadrivariant assemblages in the NCFM(Fe_2O_3)AS system. Five-phase bivariant subassemblages in the NCFMAS system are indicated by a label for the missing phase in brackets. Four-phase bivariant subassemblages in the CFMAS system are indicated by labels for the two missing phases in brackets. Dashed curves parallel to curves (CPX) and (OPX) indicate the displacement of these curves due to the addition of ferric iron-bearing components to the assemblages. The mole fraction of Fe_3O_4 component in spinel is used as a measure for this addition. The three curves correspond to mole fractions of Fe_3O_4 in spinel of 0.02, 0.04, and 0.06. Symbols on the right of this figure represent microprobe data from low-variance garnet-bearing assemblages from Westport, N.Y. The symbols ▲, ★, ✪, □, and ● represent the mole fractions of $Ca_3Al_2Si_3O_{12}$ and MgFe exchange potentials (as measured by olivine composition, X_{FA}) of garnets in the assemblages orthopyroxene–spinel–garnet, olivine–spinel–garnet–plagioclase, clinopyroxene–spinel–garnet–plagioclase, and garnets in coronas cored by orthopyroxene, olivine, and plagioclase, and clinopyroxene, olivine, and plagioclase, respectively. Significance of arrow brackets outlined in text. (B) Calculated diagram showing the mole fraction of $CaAl_2Si_2O_8$ in plagioclase (X_{AN}) as a function of FeMg exchange potential as measured by olivine composition for bi- and trivariant subassemblages of the six-phase assemblage olivine–orthopyroxene–clinopyroxene–spinel–garnet–plagioclase in the NCFMAS system and tri- and quadrivariant subassemblages in the NCFM(Fe_2O_3)AS system. Triangles show the phase relations of quadrivariant subassemblages in the NCFMAS system as they appear in the R_2O_3 plane (Al_2O_3' (A) –$CaSiO_3'$ (CS) – $MgSiO_3$ (MS)) after combining the components FeO and MgO, $CaAl_2Si_2O_8$ and $NaAlSi_3O_8$, and $NaAlSi_2O_6$. Plotting coordinates are given by the following expressions:

$$CaSiO_3' = (2CaO + 6Na_2O + FeO + MgO - SiO_2)$$
$$MgSiO_3' = (MgO + FeO)$$
and
$$Al_2O_3' = (Al_2O_3 + CaO + 5Na_2O + FeO + MgO - SiO_2).$$

[4] Although the H_2O fugacities that prevailed during the metamorphism recorded here cannot be determined due to the absence of mineral assemblages defining the chemical potential of H_2O in the skarns and country rocks, it may be inferred that $P_{H_2O} << P_{Total}$. This is suggested by calculations of f_{H_2O} in orthogneisses from the Adirondack highlands (for example, Bohlen, Peacor, and Essene, 1980) and by the fact that these skarns are about an order of magnitude thinner than blackwall type skarns for which temperatures were several hundred degrees lower but where the presence of a fluid phase was likely during metamorphism (for example, Sanford, ms).

as opposed to intracrystalline diffusion is a rate-controlling reaction step. (2) The skarn next to the quartz vein illustrates that SiO_2 may behave as an inert component relative to MgO and FeO, and that $AlO_{3/2}$ despite its relatively inert behavior, may establish smooth chemical potential gradients across reaction skarns where solid solution phases may incorporate variable quantities of aluminous components. Inert behavior of SiO_2 relative to FeO and MgO is consistent with the highly irregular interface between the inner orthopyroxene zone and the quartz vein as opposed to interface (1). The deduced mobilities of components, FeO > MgO > SiO_2, contrast sharply with those generally inferred for blackwall skarns (Sanford, 1978; Curtiss and Brown, 1969; Phillips and Hess, 1936) or experimentally produced reaction skarns in the system MgO–SiO_2–H_2O (Ildefonse and Gabis, 1976; Brady, 1977). These studies have established that SiO_2 behaves as a more mobile component than either MgO or FeO at higher activities of H_2O than those that were likely to have prevailed during the metamorphism of the orthopyroxene-bearing reaction skarns. It is likely that these differences reflect a more marked dependence of solubility of Si-bearing species such as $Si(OH)_4$ on H_2O activity than do Fe- and Mg-bearing species. (3) The orthopyroxene-bearing skarns illustrate that Fe-Mg zoning, even in minerals with relatively large interdiffusion coefficients as olivine, may be preserved in high grade, regionally metamorphosed rocks where chemical potential gradients are extreme. The zoning patterns described here may be contrasted with homogeneous chemical patterns reported for most granulites or those produced by localized retrograde cation exchange between adjacent minerals (compare Lasaga, 1977). Further understanding of the implications of the mineral zoning patterns described here may come from a more detailed study of chemical zoning of minerals as a function of grain size and location within the reaction skarn adjacent to the quartz vein.

ACKNOWLEDGMENTS

This paper represents part of my Ph.D. thesis at Harvard University. I thank David Walker for providing the extra muscle needed to collect some of the skarns, C. Bruton, S. K. Dobos, W. E. Glassley, J. F. Hays, K. Jackson, M. L. Rivers, D. Rumble III, G. Smith III, and J. B. Thompson Jr. for their comments, discussions, and reviews, and especially R. Joesten for his very extensive, constructive review of an earlier version of this manuscript.

Appendix I

Calculation of chemical potential gradients

The potential differences $\Delta\mu_{FeO}$, $\Delta\mu_{MgO}$, and $\Delta\mu_{SiO_2}$ were calculated from expressions (14) to (16). The value of the term $\Delta\mu_1^\circ$ for the endmember reaction

$$Fe_2Si_2O_6 = SiO_2 + Fe_2SiO_4 \qquad \text{(AI-1)}$$

was estimated based on the experimental data of Smith (1971), the P–T–X calibration of Wood and Strens (1971), and assemblages in rocks which record local equilibration conditions similar to those deduced here. In terms of these calculated quantities, the contributions of errors in the quantity $\Delta\mu_1^\circ$ determined by this method are negligible compared with those stemming from uncertainties in the mixing properties of orthopyroxenes and olivines. Although, based on presently available data, a strict error

analysis is impossible because it is assumption dependent, the magnitude of uncertainties in these quantities may be illustrated by choosing three sets of possible bounding assumptions for their mixing properties.

Based on (1) the experimental data of Smith (1971), (2) the P–T–X calibration of Wood and Strens (1971), (3) the compositions reported by Jaffe, Robinson, and Tracy (1978), and (4) Mg-Fe partitioning data obtained from natural quartz–orthopyroxene–olivine assemblages by Bonnichsen (1969) and Smith (1971), the following composition limits for orthopyroxene and olivine in the three phase assemblage were deduced for the temperatures (700°-760°C) and pressures (7-9 kb) of local equilibration estimated for the Westport rocks: $0.85 < X_{Fe_2Si_2O_6,\ OPX} < 0.91$ and $0.935 < X_{Fe_2SiO_4,\ OL} < 0.965$. If we assume a temperature of 730°C, ideal solid solution of both olivine and orthopyroxene, and allow for an additional uncertainty of 0.02 $X_{Fe_2SiO_4,\ OL}$, the difference $\Delta\mu_i^o$ will be between −0.150 and −0.420 kcal/gfw. Due to the iron-rich nature of both the olivines and orthopyroxenes in this three-phase assemblage, these results will not be changed significantly if mixing in olivine and orthopyroxene is nonideal. The values of $\Delta\mu_{FeO}$, $\Delta\mu_{MgO}$, and $\Delta\mu_{SiO_2}$ computed from eqs (14) to (16), assuming ideal solid solution in both olivine and orthopyroxene, are consistent with inequality (8):

$$(\Delta\mu_{FeO} = -0.33 \pm 0.14) < (-\Delta\mu_{SiO_2} = +0.62 \pm 0.14) < (\Delta\mu_{MgO} = +1.138 \pm 0.19 \text{ kcal/gfw}) \quad \text{(AI-2)}$$

Alternatively, nonideality of mixing of pyroxene due to ordering of Fe^{2+} and Mg^{2+} between M1 and M2 sites may be considered.

Based on the data of Virgo and Hafner (1969), Saxena and Ghose (1971), and Matsui and Nishizawa (1974), it may be shown that at 1000°C and for olivines with Fe/(Fe + Mg) ratios between 0.4 and 0.9, the composition dependence of the coefficient for Fe-Mg exchange between olivine and orthopyroxene may be described adequately treating olivine as an ideal solid solution and, for orthopyroxene, adding only a configurational correction to the ideal formulation to account for ordering of Fe^{2+} and Mg^{2+} between M1 and M2 sites. Based on the data of Saxena and Ghose (1971) a configurational correction alone gives the alternate result for 730°C:

$$(\Delta\mu_{FeO} = +0.20 \pm 0.14) < (-\Delta\mu_{SiO_2} = +1.40 \pm 0.14) < (\Delta\mu_{MgO} = +2.37 \pm 0.19 \text{ kcal/gfw}). \quad \text{(AI-3)}$$

However, a configurational correction alone is not adequate to describe the composition dependence of the coefficient for Fe-Mg exchange even between only olivine and orthopyroxenes of intermediate and high Fe/Mg ratios at 730°C. At temperatures between 700° and 760°C, the distribution coefficient for Fe-Mg exchange between olivine and orthopyroxene, as defined in (21), varies from roughly 1.4 (Fo_{55-60}, Westport locality) for intermediate olivines to between 2.5 and 2.7 for iron-rich olivine, (Fo_{10}) (Bonnichsen, 1969). The intersite data for orthopyroxene (Saxena and Ghose, 1971) interpolated to 730°C will account for only a variation from 2.25 to 2.6 for this range of olivine compositions. The remainder of the composition dependence of the distribution coefficient for Fe-Mg exchange between olivine and orthopyroxene may be ascribed primarily to nonconfigurational Gibbs energy terms

$$_{OPX}\Delta\overline{G}_x^\circ = \overline{G}^\circ_{(Fe)_{M2}(Mg)_{M1}Si_2O_6} + \overline{G}^\circ_{(Mg)_{M2}(Fe)_{M1}Si_2O_6} - \overline{G}^\circ_{Mg_2Si_2O_6} - \overline{G}^\circ_{Fe_2Si_2O_6} \quad \text{(AI-4)}$$

$$_{OL}\Delta\overline{G}_x^\circ = \overline{G}^\circ_{(Fe)_{M2}(Mg)_{M1}SiO_4} + \overline{G}^\circ_{(Mg)_{M2}(Fe)_{M1}SiO_4} - \overline{G}^\circ_{Mg_2SiO_4} - \overline{G}^\circ_{Fe_2SiO_4} \quad \text{(AI-5)}$$

At 730°C with the effects of these bonding terms included in the estimates of the thermodynamic mixing properties (Sack, 1980a), mixing properties of Fe-Mg olivines and orthopyroxenes may be adequately described by the empirical binary (1-2) regular solution formulation (for example, Thompson, 1967) for which

$$\overline{G}^{EX} = X_1X_2W_G \ . \quad \text{(AI-6)}$$

Allowing for an error in estimates of W_G^{OPX} of ± 0.6 kcal, an error on W_G^{OL} consistent with the error bounds on W_G^{OPX} and the composition dependence of the olivine-orthopyroxene Fe-Mg distribution coefficient, and calculating activity coefficients according to the expression

$$RT \ln \gamma_i = (1 - X_i)^2 W_G \ , \quad \text{(AI-7)}$$

the following estimates are obtained for the quantities $\Delta\mu_{FeO}$, $\Delta\mu_{MgO}$, and $\Delta\mu_{SiO_2}$:

$$(\Delta\mu_{FeO} = +0.70 \pm 0.25) < (-\Delta\mu_{SiO_2} = +1.90 \pm 0.25) < (\Delta\mu_{MgO} = +2.80 \pm 0.30 \text{ kcal/gfw}) \quad \text{(AI-8)}$$

The chemical potential paths of FeO, MgO, and SiO_2 were calculated using expressions (12) and (13) and the assumption that the chemical potential of FeO has a linear gradient between interfaces (1) and (2).

The chemical potential path of Al_2O_3 across the reaction skarn adjacent to the quartz vein was calculated from the expression

$$\Delta\mu_{Al_2O_3} = RT \ln \left[\frac{<^1>X_{Al,\,M1}}{<^b>X_{Al,\,M1}} \right] \left[\frac{<^1>X_{Mg,\,M2}\ \ <^b>X_{Mg,\,M1}}{<^1>X_{Mg,\,M1}\ \ <^b>X_{Mg,\,M2}} \right]^{(1/2)} \quad \text{(AI-9)}$$

where $<^b>$ refers to any particular point within the orthopyroxene-bearing reaction skarn. This expression was derived by subtraction of two relations of the type

$$\mu_{Al_2O_3,\,OPX} = {}^*\mu_{Al_2O_3} + RT \ln (X_{Al,\,M1}) \left(\frac{X_{Mg,\,M2}}{X_{Mg,\,M1}} \right)^{(1/2)} \quad \text{(AI-10)}$$

in which it is assumed (1) that ordering of Al^{3+} in SiB and M1 sites is complete in accordance with the crystallographic observations of Ganguly and Ghose (1979) and Takeda (1972), (2) that Al_2O_3 obeys Henry's Law in the range of compositions encountered, and (3) that mixing of endmember pyroxene components $Fe_2Si_2O_6$ and $Mg_2Si_2O_6$ is ideal, and where ${}^*\mu_{Al_2O_3}$ $(= {}^*\mu_{MgAl_2SiO_6,\,OPX} - \frac{1}{2}\,\mu^\circ_{Mg_2Si_2O_6,\,OPX})$ is the Henry's Law constant. $<^1>\mu_{Al_2O_3} - <^2>\mu_{Al_2O_3}$ defined by expression (AI-10) is at least 7.3 ± 0.3 kcal, the value obtained assuming ferric iron is absent in orthopyroxene and $X_{Al_{2*}}^{M1} = 0.002$ at interface (2).

Only rather general statements about the chemical potential paths of CaO and TiO_2 can be made based on the zoning patterns of CaO in orthopyroxene (see fig. 5) and the presence of ilmenite through zones between interface (1) and the initial contact surface. The chemical potential difference $\Delta\mu_{CaO}$ may be deduced from the expression

$$\Delta\mu_{CaO} = \Delta\mu_{Ca\overline{Fe}} + \Delta\mu_{FeO} \quad \text{(AI-11)}$$

where the chemical potential path of the exchange component $Ca\overline{Fe}$, like that of $Mg\overline{Fe}$ and Al_2O_3, may be defined continuously throughout the reaction skarn. The chemical potential path of $Ca\overline{Fe}$ was deduced from the expression

$$\Delta\mu_{Ca\overline{Fe}} = RT \ln \left(\frac{X_{Ca,\,M2}}{X_{Fe,\,M2}} \right) - RT \ln \left(\frac{<^1>X_{Ca,\,M2}}{<^1>X_{Fe,\,M2}} \right) \quad \text{(AI-12)}$$

in which Henry's Law behavior is assumed for $CaFeSi_2O_6$ in orthopyroxene, partitioning of Fe^{2+} and Mg^{2+} between M1 and M2 sites is taken into account, and $<^1>$ refers to interface (1). Corresponding to the pattern of calcium variations in pyroxenes, the chemical potential path of $Ca\overline{Fe}$ exhibits a maximum at interface (2) (see fig. 5). Other features of the calculated path may not be significant in view of the uncertainties in the probe data and calculation procedure. Even less definite statements can be made about the chemical potential path of TiO_2. Between interface (1) and the margin of the zone composed almost entirely of orthopyroxene, the chemical potential profile of TiO_2 is the mirror image of that of FeO due to the presence of ilmenite of essentially constant composition and the relationship

$$\mu_{FeTiO_3,\,ILM} = \mu_{TiO_2} + \mu_{FeO} \quad \text{(AI-13)}$$

Beyond this margin it cannot be defined with any certainty due to the dilute nature of Ti-bearing mineral components in orthopyroxene and the only rare presence of ilmenite.

Appendix 2

Non-MFS mineral reactions

There are two objectives of this appendix. Its first objective is to outline the non-MFS reactions that have contributed to the present distribution of assemblages and zoning patterns within the skarns. Its second objective is to document that inferences based solely on the analysis of Fe-Mg zoning in the olivine–orthopyroxene–quartz sub-

system of the skarns are consistent with deductions based on analysis of mineral assemblages and associated patterns of disequilibrium within the larger systems comprised by the skarns and the country rocks. For these purposes, non-MFS reactions are conveniently divided into two groups. These are garnet-forming reactions and reactions that preceded garnet-forming reactions.

Although it is possible to enumerate many types of garnet-forming reactions, only two such reactions will be considered here. The first of these illustrates the effects garnet growth may have had on zoning patterns established during initial growth of the inner zone of the skarn next to the dike. The second of these places constraints on the phase relations among the minerals olivine, orthopyroxene, clinopyroxene, spinel, garnet, plagioclase in the NCFMAS system at the conditions of local metamorphic equilibration.

Because garnet has a greater Fe/Mg ratio than other phases from which it can form in the system CFMAS, growth of garnet within the inner zone of the skarn adjacent to the dike may have erased an inner iron-enrichment pattern within it, providing components had lower diffusivities during garnet growth than they had at the time of initial growth of this skarn. The possibility that an inner iron-enrichment pattern was established in the inner zone of this skarn prior to local metamorphic equilibration is suggested by the present makeup of this zone, orthopyroxene and garnet, as well as by the isolated grains of orthopyroxene within the outer margin of the dike which exhibit an increase in Fe/(Fe + Mg) from 0.34 at the dike margin to about 0.45 2 mm to the inner side of the inner interface. This may be illustrated by considering the reaction that led to the production of this zone. Assuming that the initial composition of plagioclase in the dike was approx $An_{19}(Ab + Or)_{81}$ (the average composition of plagioclase adjacent to the reaction skarn at present), then, taking into account the volumetric proportions and compositions of orthopyroxene and garnet in this zone, making the assumption that Al_2O_3 behaves as an inert component, and again combining MgO, FeO, and MnO as one component, MFO, this reaction may be written as

$$\underset{\text{plagioclase}}{Ca_{0.19}(Na + K)_{0.81}Al_{1.19}Si_{2.81}O_8} + 1.55\ \underset{\text{quartz}}{SiO_2} + 0.06\ CaO + 4.12\ FMO = 2.48\ \underset{\text{orthopyroxene}}{Ca_{0.1}FM_{1.66}Si_{1.79}O_6} + \underset{\text{garnet?}}{0.41\ (Na + K)_2O} \qquad \text{(AII-1)}$$

In this reaction it is not possible to specify the initial proportions of orthopyroxene and garnet in this zone because these may be adjusted continuously by the isochemical reaction

$$\underset{\text{orthopyroxene}}{(MF)_2Si_2O_6} + \underset{}{(MF)Al_2SiO_6} = \underset{\text{garnet}}{(MF)_3Al_2Si_3O_{12}} \qquad \text{(AII-2)}$$

in response to changes of temperature and pressure. Assuming approximately isochemical replacement of orthopyroxene by garnet due to this reaction, orthopyroxenes in this zone would have become more magnesian because garnet has a greater Fe/Mg ratio than coexisting orthopyroxene. Such replacement could have erased an earlier inner iron-enrichment pattern in this zone.

To test the plausibility of this assumed mechanism it is instructive to compare the average Fe/(Fe + Mg) ratio of the inner zone of the skarn with that of orthopyroxenes 2 mm to the inner side of the inner interface. These pyroxenes have about the same Fe/(Fe + Mg) ratio as the average Fe/(Fe + Mg) ratio of the inner zone, 0.45, but are much less aluminous than the orthopyroxenes in contact with garnet in the inner zone of the skarn. In addition, since the gradient in μ_{MgFe} between the inner interface and the orthopyroxenes in the dike is an order of magnitude larger than other such gradients in either skarn, it is likely that prior to metamorphic equilibration of local assemblages considerable replacement of orthopyroxene by garnet occurred in the inner zone of the skarn adjacent to the dike. A completely secondary metamorphic origin for the garnet in this zone might be considered questionable, however, because this would imply considerable changes in pressure-temperature conditions between the time of the initial growth of the skarn and final metamorphic equilibration of local assemblages. If garnet were entirely secondary, during the initial growth of this zone the pyroxenes would have been about 4.5 times more aluminous than they are at present. Based on calibrations of the alumina content of orthopyroxene coexisting with garnet in the system CFMAS (Wood and Banno, 1973; Wood, 1974; Akella, 1976) this would imply that relative to the conditions of local metamorphic equilibration (730 ± 50°C and 8 ± 1 kb) temperature-pressure changes were within the two limiting bounds: (1) a

decrease in temperature of about 300°C at constant pressure, and (2) an increase in pressure of greater than 5 kb at constant temperature.

Although it may be difficult to establish a completely secondary metamorphic origin for the garnet in the inner zone of the skarn next to the dike, such an origin may be established readily for the rest of the garnet in both skarns. In similar fashion to the case discussed above, garnet mineralization in the skarn adjacent to the quartz vein may have led to the erasure of an iron-enrichment pattern in the outer portion of this skarn. Within this portion of this skarn, as well as the corresponding portion of the other skarn, garnet growth was controlled by a CFMAS analog of the MAS reaction

$$\underset{\text{spinel}}{(1-2x)\,MgAl_2O_4} + \underset{\text{orthopyroxene}}{2\,Mg_{(2-x)}Al_{2x}Si_{(2-x)}O_6} = \underset{\text{garnet}}{Mg_3Al_2Si_3O_{12}} + \underset{\text{olivine}}{(1-2x)Mg_2SiO_4} \qquad \text{(AII-3)}$$

Evidence for a CFMAS analog of this reaction is recorded by the development of (A) the three-phase assemblages spinel–garnet–olivine and orthopyroxene–olivine–garnet at interface (1) in the skarn adjacent to the dike and (B) the assemblage olivine–spinel–orthopyroxene at interface (1) in the skarn adjacent to the quartz vein. Although extrapolation of experimental data suggest that at 739°C this reaction occurs at about 18 kb in the MAS system (Danckwerth and Newton, 1978; Herzberg, 1978; Obata, 1976), the reaction boundary is shifted to lower pressures at a given temperature with progressive exchange along the exchange vectors $Ca\overline{Mg}$ (that is, Ca^{2+} –Mg^{2+}) and $Mg\overline{Fe}$ because these exchanges are more extensive in the products than in the reactants of (AII-3). Within the outer portions of the skarns where spinel was stable prior to garnet growth, the reaction boundary was further stabilized relative to interface (1) due to the lower values of $\mu_{Mg_2SiO_4}$ within the skarns. Thus we may infer that in the reaction skarn adjacent to the quartz vein, garnet growth began at about 0.55 cm to the inner side of interface (1) and proceeded to within about 0.5 mm of this interface. Within this portion of the skarn a CFMAS analog of expression (AII-3) is not an appropriate description of the garnet-forming reaction, however, because olivine was not stable here. For the observed mineral compositions the garnet-forming reaction within this skarn was

$$\underset{\text{spinel}}{FMAl_2O_4} + 1.71\,\underset{\text{orthopyroxene}}{Ca_{0.015}FM_{1.925}Al_{0.12}Si_{1.92}O_6} + 0.4\,CaO = 1.10\,\underset{\text{garnet}}{(Ca_{0.13}FM_{0.87})_3Al_2Si_3O_{12}} + 1.42\,FMO \qquad \text{(AII-4)}$$

assuming SiO_2 behaved as an inert component relative to FMO and CaO. Because garnet growth did not progress all the way to interface (1), the point of appearance of garnet within this skarn provides a natural reversal for the extent of $Ca\overline{Mg}$ and $Fe\overline{Mg}$ exchanges which must be made to a spinel–orthopyroxene–garnet–olivine assemblage initially in the MAS system, to stabilize it to the conditions of local metamorphic equilibration recorded here.

It is instructive to compare the bounds suggested above with those determined from the composition data from local assemblages within the surrounding rocks (Sack, 1977, 1980b). In the CFMAS system the four-phase assemblage spinel–orthopyroxene–garnet–olivine is trivariant. Hence at a given temperature, pressure, and mole fraction of $Ca_3Al_2Si_3O_{12}$ in garnet ($\backsim$0.13 in the skarn), the olivine composition in the four-phase assemblage is uniquely determined.[5] Thus the composition of olivine in the three-phase assemblage olivine–spinel–orthopyroxene at interface (1) places a minimum bound on the Fe/(Fe + Mg) ratio required to develop the four-phase assemblage; a maximum bound on this ratio may be obtained by taking into account the lower value of $\mu_{Mg_2SiO_4}$ at the point of appearance of garnet relative to that defined by olivine at interface (1). In figure 7 these bounds are compared with the phase relations among bi- and trivariant subassemblages of the six-phase assemblage olivine–orthopyroxene–clinopyroxene–spinel–garnet–plagioclase in the NCFMAS system and subsystems at 730 ± 50°C and 8 ± 1 kb. The agreement between these brackets and the location of the composition curve for the five-phase assemblage olivine–spinel–orthopyroxene–garnet–plagioclase (CPX) determined from the country rocks demonstrates that the garnet-

[5] The assemblages in the skarns depart from the CFMAS system principally by the additions of small amounts of Cr_2O_3, MnO, and Fe_2O_3. Although these additions raise the variance of these assemblages, they do not alter the systematics presented here because they are readily taken into account. See caption of figure 7 for further clarification.

forming reactions in the skarns parallel those in the country rocks and, thus, proves that the skarns were formed prior to Grenville metamorphic equilibration.[6] In addition, because the composition of garnet in the three-phase assemblage garnet–orthopyroxene–clinopyroxene is relatively insensitive to temperature and pressure, typically between 0.16 and 0.20 $X_{Ca_3Al_2Si_3O_{12},\ GAR}$ (Thompson, 1979, Sack, 1980b), these brackets effectively demonstrate that given an appropriate bulk composition, the full six-phase assemblage may be stably developed over a range of temperature and pressure conditions characteristic of the lower crust. Further, because the composition isopleths of the binary solid solutions olivine and plagioclase have large angles of intersection over most of the stability range of this assemblage (Sack, 1980b), it is an ideal reference for outlining the fine structure of the gabbro-eclogite transformation and examining the petrogenetic significance of garnet-bearing corona structures and associated patterns of chemical disequilibrium in quartz-undersaturated rocks. Sack has used these isopleths and patterns of disequilibrium in the country rocks to show that possible paths of local metamorphic equilibration were bounded as follows: (1) $dT/dh > 90°/km$ for $dT < 0$ and $dP < 0$, (2) $dT/dh < 16°/km$ for $dT > 0$, or (3) $dT/dh < 0$ for $dP > 0$ (where $dP = \rho g dh$).

In addition to garnet-forming reactions and reactions within an endmember MFS skarn, reactions involving the alteration of plagioclase feldspar and magnetite are required to acount for the present distribution of assemblages and zoning patterns in the skarns. In the skarn next to the vein magnetite breakdown reactions are required to explain the absence of magnetite in the plagioclase–orthopyroxene–ilmenite zone to the outer side of the initial interface. The conversion of magnetite to ilmenite in these zones may be represented by the reaction

$$\left[x - \left(\frac{1-x}{1-y}\right) y \right] H_2 + [xFe_3O_4 + (1-x)Fe_2TiO_4] = \left[x - \left(\frac{1-x}{1-y}\right) y \right] H_2O + \left[1 + 2\left(x - \left(\frac{1-x}{1-y}\right) y \right)\right] FeO + \left(\frac{1-x}{1-y}\right) \left[(1-y)FeTiO_3 + yFe_2O_3 \right] \quad \text{(AII-5)}$$

magnetite SS; ilmenite SS

where x and y are the mole fractions of Fe_3O_4 and Fe_2O_3 components in magnetite and ilmenite solid solutions. This reaction together with the oxidation reaction

$$\underset{\text{ulvospinel}}{Fe_2TiO_4} = \underset{\text{ilmenite}}{FeTiO_3} + FeO \quad \text{(AII-6)}$$

provides mechanisms for generating FeO needed for mass-balance within the inner orthopyroxene zone and producing core to rim iron-enrichments of orthopyroxenes near interface (2) in both skarns.

The present distributions of biotite and hornblende within the skarn next to the quartz vein suggests that $AlO_{3/2}$ and SiO_2 behaved as inert components relative to CaO, FMO, alkali, and volatile components during feldspar alteration reactions.. For the assumptions that $AlO_{3/2}$, TiO_2, and SiO_2 behave as inert components relative to these latter components, feldspar replacement reactions leading to the production of biotite and spinel in zones bordering interface (1) of the orthopyroxene-bearing reaction skarns may be approximated by linear combinations of endmember reactions

$$\underset{\text{albite}}{NaAlSi_3O_8} + KO_{1/2} + 3FMO + (H_2O, F_2, Cl_2) = \underset{\text{biotite}}{KFM_3Al_2Si_2O_{10}(OH, Cl, F)_2} + NaO_{1/2} \quad \text{(AII-7)}$$

$$\underset{\text{albite}}{NaAlSi_3O_8} + KO_{1/2} + \underset{\text{ilmenite}}{FMTiO_3} + FMO + (H_2O, F_2, Cl_2) = \underset{\text{biotite}}{K(FM_2Al_{0.5}Ti_{0.5})AlSi_2O_{10}(OH, Cl, F)_2} + NaO_{1/2} \quad \text{(AII-8)}$$

[6] In the NCFMAS system the composition curves for the four-phase assemblage spinel–orthopyroxene–garnet–olivine (CPX, PLAG) and the five-phase assemblage (CPX) are identical because both assemblages are effectively trivariant due to only negligible substitution of Na_2O-bearing components in all minerals but plagioclase.

$$1.17\ \underset{\text{anorthite}}{CaAl_2Si_2O_8} + KO_{1/2} + 2.33\ FMO + (H_2O, F_2, Cl_2) = \underset{\text{biotite}}{KFM_{2.33}Al_{2.33}Si_{2.33}O_{10}(OH, Cl, F)_2} + 1.17\ CaO \quad \text{(AII-9)}$$

and

$$3\ \underset{\text{anorthite}}{CaAl_2Si_2O_8} + 2\ FMO + 2\ NaO_{1/2} = 2\ \underset{\text{albite}}{NaAlSi_3O_8} + 2\ \underset{\text{spinel}}{FMAl_2O_4} + 3\ CaO \quad \text{(AII-10)}$$

Potassium required for biotite was derived from components introduced with the dike and vein or by $K\overline{Na}$ exchange with feldspar. In the reaction skarn next to the quartz vein $NaO_{1/2}$ liberated from reactions in the vicinity of interface (1) was used to generate progressively more sodic feldspars between interface (1) and (2). This was accomplished through (AII-10) or the reaction

$$2\ NaO_{1/2} + \underset{\text{anorthite}}{CaAl_2Si_2O_8} + 2\ \underset{\text{orthopyroxene}}{FM_2Si_2O_6} = 2\ \underset{\text{albite}}{NaAlSi_3O_8} + CaO + 2\ FMO \quad \text{(AII-11)}$$

after a point at which spinel was no longer stable due to increased activity of SiO_2. In the plagioclase–orthopyroxene–ilmenite zone near the initial interface this latter reaction further reduced the modal orthopyroxene/plagioclase ratio relative to that due to (21). CaO liberated in reactions (AII 9-11) was combined with FMO and SiO_2 (quartz) to form orthopyroxenes at interface (2). Most of the CaO liberated in these reactions, however, was consumed in the reaction

$$CaO + \underset{\text{orthopyroxene}}{FM_2Si_2O_6} = \underset{\text{clinopyroxene}}{CaFMSi_2O_6} + FMO \quad \text{(AII-12)}$$

to widen the narrow zone of clinopyroxene (+ orthopyroxene) next to the initial contact. The set of reactions (21) (AII 5-12) plus the reaction

$$FMO + \underset{\text{quartz}}{SiO_2} = 1/2\ \underset{\text{orthopyroxene}}{FM_2Si_2O_6} \quad \text{(AII-13)}$$

an analogous intrazone exchange and precipitation reaction may be combined to yield balanced chemical reactions describing widening of the reaction skarn next to the quartz vein prior to secondary metamorphic mineralization of garnet. In addition, hornblende reaction relations must be added to the above list to account for more details of the skarns.

Although a comprehensive treatment of hornblende reactions is beyond the bounds of this discussion, it is instructive to consider briefly the pattern of hornblende mineralization within the reaction skarn adjacent to the quartz vein in light of our assumptions that $AlO_{3/2}$, TiO_2, and SiO_2 may be treated as inert components relative to FMO, CaO, alkali, and volatile components. The pattern of hornblende mineralization within this skarn appears to support this assumption. Hornblende is of variable composition, but all hornblende analyses obtained have an Al/Si ratio greater than 1/3, that of albite component. If both $AlO_{3/2}$ and SiO_2 behave as inert components relative to these other components, hornblende stability would be limited by plagioclase composition because the TiO_2 percentages are comparable in the plagioclase–orthopyroxene–ilmenite and hornblende–orthopyroxene zones. This would account for the observation that hornblende is not usually present in the albitic portion of the compositionally zoned plagioclase reservoir between interfaces (1) and (2) in this skarn. However, this could also reflect the limits of hornblende stability (for example, Glassley and Sorensen, 1980).

References

Akella, J., 1976, Garnet pyroxene equilibria in the system $CaSiO_3$–$MgSiO_3$–Al_2O_3 and in a natural mineral mixture: Am. Mineralogist, v. 61, p. 589-598.

Albee, A. L. and Ray, L., 1970, Correction factors for electron microprobe microanalysis of silicates, oxides, carbonates, phosphates, and sulfates: Anal. Chem., v. 42, p. 1408-1414.

Barker, F., 1964, Reaction between mafic magmas and pelitic schist, Cortlandt, New York: Am. Jour. Sci., v. 262, p. 614-634.

Bence, A. E. and Albee, A. L., 1968, Empirical correction factors for the electron microanalysis of silicates and oxides: Jour. Geology, v. 76, p. 382-403.

Bohlen, S. R., Boettcher, A. L., and Essene, E. J., 1978, Experimental reinvestigation of ferrosilite–fayalite–quartz stability [abs.]: EOS, v. 59, p. 402.

Bohlen, S. R. and Essene, E. J. 1980, Evaluation of coexisting garnet-biotite, garnet-clinopyroxene, and other Fe-Mg exchange thermometers in Adirondack granites: Geol. Soc. America Bull., v. 91, pt. 1, p. 107-109; pt. 2, p. 685-719.

Bohlen, S. R., Peacor, D. R., and Essene, E. J., 1980, Crystal chemistry of metamorphic biotite and its significance in water barometry: Am. Mineralogist, v. 65, p. 55-62.

Bonnichsen, B., 1969, Metamorphic pyroxenes and amphiboles in the biwabik iron formation, Dunka River area, Minnesota: Mineralog. Soc. America Spec. Paper 2, p. 217-239.

Brady, J. B., 1975, Reference frames and diffusion coefficients: Am. Jour. Sci., v. 275, p. 954-983.

———— 1977, Experimental reaction zones between quartz and periclase and intergranular diffusion of silica [abs.]: EOS, v. 58, p. 520.

———— 1977, Metasomatic zones in metamorphic rocks: Geochim. et Cosmochim. Acta, v. 41, p. 113-125.

Buddington, A. F. and Whitcomb, L., 1941, Geology of the Willsboro Quadrangle, New York [1:62,500]: New York State Mus. Bull. 325, 137 p.

Buening, D. K. and Buseck, P. R., 1973, Fe-Mg lattice diffusion in olivine: Jour. Geophys. Research, v. 78, p. 6852-6862.

Carmichael, D. M., 1969, On the mechanism of prograde metamorphic reactions in quartz-bearing pelitic rocks: Contr. Mineralogy Petrology, v. 20, p. 244-267.

Carswell, D. A., Curtis, C. D., and Kanaris-Sotiriou, R., 1974, Vein metasomatism in peridotite at Kalsket near Tafjord, South Norway: Jour. Petrology, v. 15, p. 383-402.

Curtis, C. D. and Brown, P. E., 1969, The metasomatic development of zoned ultrabasic bodies in Unst, Shetland: Contr. Mineralogy Petrology, v. 24, p. 275-292.

Darken, L. S., 1948, Diffusion, mobility, and their interrelation through free energy in binary metallic systems: Am. Inst. Mining Metallurg. Pet. Eng. Trans., v. 175, p. 189-201.

———— 1949, Diffusion of carbon in austenite with a discontinuity in composition: Am. Inst. Mining Metallurg. Pet. Eng. Trans., v. 180, p. 430-438.

Eugster, H. P., 1970, Thermal and ionic equilibria among muscovite, K-feldspar and aluminosilicate assemblages: Fortscher. Mineralogie, v. 47, p. 106-123.

Fisher, G. W., 1970, The application of ionic equilibria to metamorphic differentiation: an example: Contr. Mineralogy Petrology, v. 29, p. 91-103.

———— 1973, Nonequilibrium thermodynamics as a model for diffusion controlled metamorphic processes: Am. Jour. Sci., v. 273, p. 897-924.

———— 1977, Nonequilibrium thermodynamics in metamorphism, *in* Fraser, D. G., ed., Thermodynamics in Geology: Boston, D. Reidel, p. 391-403.

Fisher, G. W. and Elliot, D., 1974, Criteria for quasi-steady diffusion and local equilibrium in metamorphism, *in* Hofmann, A. W., Biletti, B. J., Yoder, H. S., Jr., and Yund, R. A., eds., Geochemical Transport and Kinetics: Washington, D.C., Carnegie Inst. Washington Pub. 634, p. 231-241.

Frantz, J. D. and Mao, H. K., 1976, Bimetasomatism resulting from intergranular diffusion: I. Theoretical model for monomineralic reaction zone sequences: Am. Jour. Sci., v. 276, p. 817-840.

Ganguly, J. and Ghose, S., 1979, Aluminous orthopyroxene: order-disorder, thermodynamics properties, and petrologic implications: Contr. Mineralogy Petrology, v. 69, p. 375-386.

Gibbs, J. W., 1928, The collected work of J. Willard Gibbs, v. 1: New Haven, Conn., Yale Univ. Press, 434 p.

Glassley, W. E. and Sorensen, K., 1980, Constant P_s–T amphibolite to granulite facies transition in Agto (West Greenland) metadolerites: implications and applications: Jour. Petrology, v. 21, p. 69-105.

deGroot, S. R. and Mazur, P., 1969, Nonequilibrium thermodynamics: Amsterdam, North Holland Pub. Co., 510 p.

Heubner, J. S., Ross, M., and Hickling, N., 1975, Significance of exsolved pyroxenes from lunar breccia 77215: Lunar Sci. Conf., 6th, Houston, Tex., Proc., p. 529-546.

Ildefonse, J.-P. and Gabis, V., 1976, Experimental study of silica diffusion during metasomatic reactions in the presence of water at 550°C and 1000 bars: Geochim. et Cosmochim. Acta, v. 40, p. 297-303.

Jaffe, H. W., Robinson, Peter, and Tracy, R. J., 1978, Orthoferrosilite and other iron-rich pyroxenes in microperthite gneiss of the Mount Marcy area, Adirondack Mountains: Am. Mineralogist, v. 63, p. 1116-1136.

Joesten, R., 1974, Local equilibrium and metasomatic growth of zoned calcsilicate nodules from a contact aureole, Christmas Mountains Big Bend region, Texas: Am. Jour. Sci., v. 274, p. 876-901.

———— 1977, Evolution of mineral assemblage zoning in diffusion metasomatism: Geochim. et Cosmochim. Acta, v. 41, p. 649-670.

Johnson, B. L. and Warren, C. H., 1908, Contributions to the geology of Rhode Island: I. Notes on the history and geology of Iron Mine Hill, Cumberland; II. The petrography and mineralogy of Iron Mine Hill, Cumberland: Am. Jour. Sci., v. 25, p. 1-38.

Kemp, J. F., 1894, Gabbros on the western shore of Lake Champlain: Geol. Soc. America Bull., v. 5, p. 213-234.

Korzhinskii, D. S., 1959, Physiochemical basis of the analysis of the paragenesis of minerals: New York, Consultants Bur., Inc., 142 p.

Lasaga, A. C., Richardson, S. M., and Holland, H. D., 1977, The mathematics of cation diffusion and exchange between silicate minerals during retrograde metamorphism, *in* Saxena, S. K. and Bhattacharji, S., eds., Energetics of Geological Processes: New York, Springer-Verlag, p. 353-388.

Matsui, Y. and Nishizawa, O., 1974, Iron (II)-magnesium exchange equilibrium between olivine and calcium-free pyroxene over a temperature range 800°C to 1300°C: Soc. franç minéralogie cristallographie Bull., v. 97, p. 122-130.

Orville, P. M., 1969, A model for metamorphic differentiation origin of thin-layered amphibolites: Am. Jour. Sci., v. 267, p. 64-86.

Phillips, A. H. and Hess, H. H., 1936, Metamorphic differentiation at contacts between serpentinite and siliceous country rocks: Am. Mineralogist, v. 21, p. 333-362.

Read, H. H., 1931, On corundum-spinel xenoliths in the gabbro of Haddo House, Aberdeenshire: Geol. Mag., v. 68, p. 446-453.

Robie, R. A., Bethke, P. M., and Beardsley, K. M., 1967, Selected X-ray crystallographic data, molar volumes, and densities of minerals and related substances: U.S. Geol. Survey Bull. 1248, 70 p.

Sack, R. O., 1977, Spinel–garnet–plagioclase equilibria in a layered metagabbro dike from Westport, New York: Geol. Soc. America Abs. with Programs, v. 9, p. 1152.

———— ms, 1979, Studies of mafic granulites: Ph.D. thesis, Harvard Univ., 420 p.

———— 1980a, Some constraints of the thermodynamic mixing properties of Fe-Mg orthopyroxenes and olivines: Contr. Mineralogy Petrology, v. 71, p. 257-269.

———— 1980b, Adirondack mafic granulites and a model lower crust: Geol. Soc. America Bull., v. 91, pt. 1, p. 89-93; pt. 2, p. 349-442.

Sanford, R. F., ms, 1978, Regional metamorphism of ultramafic bodies and their contact zones, western New England: Ph.D. thesis, Harvard Univ., 377 p.

Saxena, S. K. and Ghose, S., 1971, Mg^{2+}-Fe^{2+} order-disorder and the thermodynamics of the orthopyroxene-crystalline solution: Am. Mineralogist, v. 56, p. 532-559.

Shay, K., 1975, Mineralogical zoning in a scapolite-bearing body on San Gorgonio Mountain, California: Am. Mineralogist, v. 60, p. 785-797.

Smith, D., 1971, Stability of the assemblage iron-rich orthopyroxene–olivine–quartz: Am. Jour. Sci., v. 271, p. 370-382.

Snetsinger, K. G., Bunch, T. E., and Keil, K., 1968, Electron microprobe analysis of vanadium in the presence of titanium: Am. Mineralogist, v. 53, p. 1770-1773.

Takeda, H., 1972, Crystallographic studies of coexisting alumian orthopyroxene and augite of high-pressure origin. Jour. Geophys. Research, v. 77, p. 5798-5811.

Thompson, A. B., 1975, Calc-silicate diffusion zones between marble and pelitic schist: Jour. Petrology, v. 16, p. 314-346.

———— 1979, Metamorphism in a model mantle: I. Prediction of P–T–X relations in $CaO–Al_2–MgO–SiO_2$, *in* Boyd, F. R. and Meyer, H. O. A., eds., The Mantle Sample: Inclusions in Kimberlites and Other Volcanics: Washington, Am. Geophys. Union, p. 15-28.

Thompson, J. B., Jr., 1959, Local equilibrium in metasomatic processes, *in* Abelson, P. H., ed., Researches in Geochemistry: New York, John Wiley & Sons, p. 427-457.

———— 1967, Thermodynamic properties of simple solutions, *in* Abelson, P. H., ed., Reserches in Geochemistry: New York, John Wiley & Sons, p. 340-361.

Thompson, J. B., Jr. and Thompson, A. B., 1976, A model system for mineral facies in pelitic schists: Contr. Mineralogy Petrology, v. 48, p. 243-277.

Vidale, R., 1969, Metasomatism in a chemical gradient and the formation of calc-silicate bands: Am. Jour. Sci., v. 267, p. 857-874.

Vidale, R. and Hewitt, D. A., 1973, "Mobile" components in the formation of calc-silicate bands: Am. Mineralogist, v. 58, p. 991-997.

Virgo, D. and Hafner, S. S., 1969, Fe^{2+}, Mg order-disorder in heated orthopyroxenes: Mineralog. Soc. America Spec. Paper 2, p. 67-81.

Weare, J. H., Stephens, J. R., and Eugster, H. P., 1976, Diffusion metasomatism and mineral reaction zones: general principles and application to feldspar alteration: Am. Jour. Sci., v. 276, p. 767-816.

Whitney, P. R. and McLelland, J. M., 1973, Origin of coronas of the Adirondack Mountains, New York: Contr. Mineralogy Petrology, v. 28, p. 81-98.

Wood, B. J., 1974, The solubility of alumina in orthopyroxene coexisting with garnet: Contr. Mineralogy Petrology, v. 46, p. 1-15.

Wood, B. J. and Banno, S., 1973, Garnet-orthopyroxene and orthopyroxene-clinopyroxene relationships in simple and complex systems: Contr. Mineralogy Petrology, v. 42, p. 109-124.

Wood, B. J. and Strens, R. G. J., 1971, The orthopyroxene geobarometer: Earth Planetary Sci. Letters, v. 11, p. 1-6.